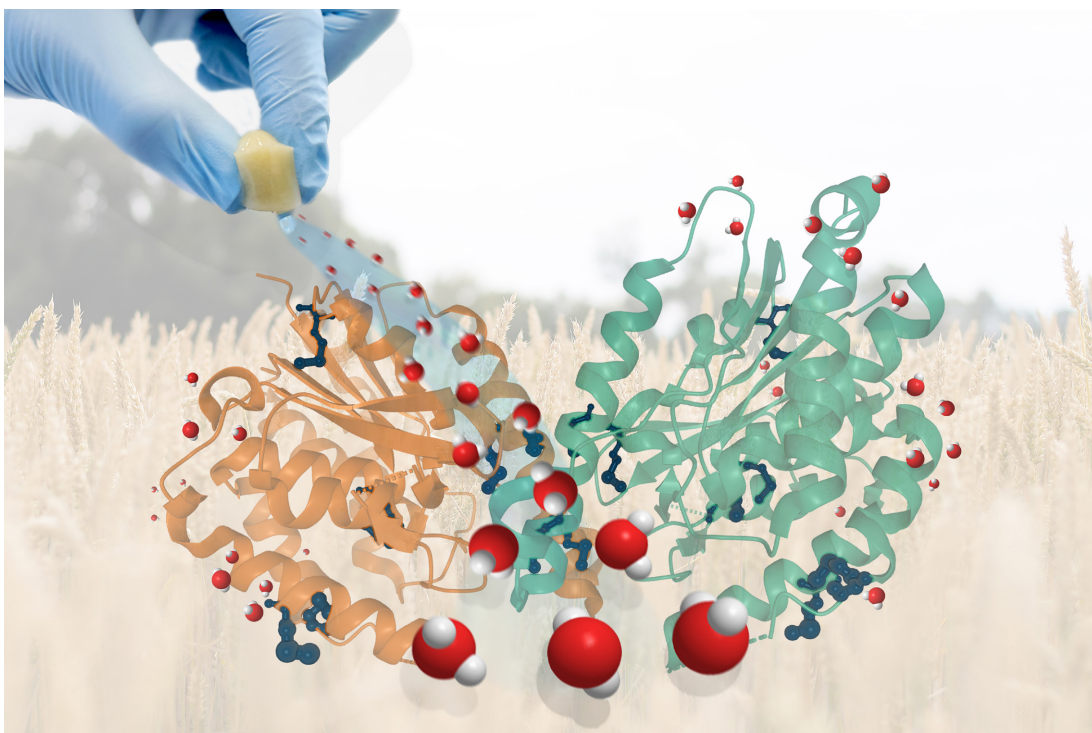


DOCTORAL THESIS

Sustainable Biobased Protein Superabsorbents from Agricultural Co-Products

ANTONIO J. CAPEZZA





Sustainable Biobased Protein Superabsorbents from Agricultural Co-Products

ANTONIO J. CAPEZZA

Academic Dissertation which, with due permission of the KTH Royal Institute of Technology and SLU Swedish University of Agricultural Sciences, is submitted for public defence for the Degree of Doctor of Philosophy on Friday the 16th of October 2020, at 9.00 a.m. in Navet, Sundsvägen 12, Alnarp.

Doctoral thesis in Product Quality and Fibre and Polymer Science.
SLU Swedish University of Agricultural Sciences; KTH Royal Institute of Technology.
Alnarp-Stockholm, Sweden 2020.

© Antonio J. Capezza, Alnarp-Stockholm, 2020

Cover design (Antonio Capezza): Wheat gluten protein gel illustrating the release of water onto a patatin protein molecule. The molecule has been retrieved from: PDB ID: 5FQU, Vinicius da Mata Madeira, P., Zouhir, S., Basso, P., Neves, D., Laubier, A., Salacha, R., Bleves, S., Faudry, E., Contreras-Martel, C., Dessen, A. (2016). Mol* (D. Sehnal, A.S. Rose, J. Kovca, S.K. Burley, S. Velankar (2018) Mol*: Towards a common library and tools for web molecular graphics MolVA/EuroVis Proceedings. doi:10.2312/molva.20181103), and RCSB PDB.

All the figures have been reproduced under permission from the publishers. Further permissions related to the material excerpted should be directed to the respective publishers.

TRITA-CBH-FOU-2020:50

ISBN (print version): 978-91-7760-624-6

ISBN (electronic version): 978-91-7760-625-3

ISSN: 1652-6880

Acta Universitatis Agriculturae Sueciae

Serial number in the Acta-series: 2020:53

Printed by: SLU Service/Repro, Alnarp 2020.

*To my beloved family, and those who
were there for me from the beginning...*

Abstract

The preparation of sustainable protein superabsorbents from agricultural industry side-streams is reported. Wheat gluten (WG), a co-product from the ethanol/starch industry, was processed into foams with sponge-like behavior and high liquid uptake. The materials were obtained by phase-separation of aqueous WG dispersions followed by ambient drying, or by lyophilization. The use of a natural and non-toxic cross-linker (genipin) resulted in foams with high water swelling properties (~18 g/g in 10 min). The rapid swelling may be of use in bio-based foams in e.g., sanitary pads.

As an alternative, potato protein concentrate (PPC, side-stream from the starch industry), was functionalized and prepared as particles. The liquid swelling capacity was compared after acylation with five different agents. It is shown that the PPC can be acylated to replicate the chemistry of synthetic superabsorbent polymers (SAP), showing water swelling capacity >10 g/g. The acylation (using EDTAD) of WG suspensions resulted in protein particles with water and saline uptake of 22 and 5 g/g, respectively. Limited network stability was however observed when acylating WG in low-protein suspensions. This was addressed by mixing the acylated protein with genipin, which provided a stable protein network. The process gave functionalized particles with swelling capacity ~40 g/g and ~80 % retention of swelling in centrifuge retention tests.

The extrusion of WG showed that porous WG with water uptake of 500 % can be produced. Further, the scalability of PPC production was pilot-tested by functionalizing potato fruit juice (PFJ), containing the potato protein in its soluble state before the industrial drying used to obtain PPC. This resulted in water swelling capacities >10 g/g, which was comparable to the PPC-functionalized materials. The results pave the way for future optimization of high-throughput production techniques using protein sources in mass production of sustainable protein-based SAPs.

Keywords proteins, circularity, superabsorbents, sustainability, acylation, extrusion.

Sammanfattning

Produktion av hållbara protein-superabsorbenter från jordbruksindustrins sidoströmmar genomfördes i denna avhandling. Vetegluten (WG), en samprodukt från etanol/stärkelseindustrin, bearbetades till skum med högt vätskeupptag. Porösa WG-material erhöles genom både fassetparation av vatten/WG-dispersioner med efterföljande torkning samt genom vakuum-torkning. Användning av en naturlig och giftfri tvärbindare (genipin) ledde till WG-skum som tog upp ~18 g vatten / g skum på 10 min. Denna egenskap gör de biobaserade skummen intressanta för t.ex. hygienkuddar (sanitary pads).

Potatisproteinkoncentrat (PPC), en sidostrom från stärkelseindustrin, funktionaliserades och svällningsförmågan undersöktes efter acylering med fem olika substanser. Det modifierade PPC efterliknade kemin hos syntetiska superabsorberande polymerer (SAP) och erhöles att vattenupptag >10 g/g. Acylering av WG i suspensionsform resulterade i proteinpartiklar med vatten- och saltlösnings-upptag på 22 respektive 5 g/g. Den begränsade stabiliteten som erhöles vid acylering av WG i utspädd form löstes genom att tillsätta genipin. Förfarandet resulterade i partiklar med en svällningskapacitet på ~40 g/g och en retention på ~80 % i centrifugeringstestet.

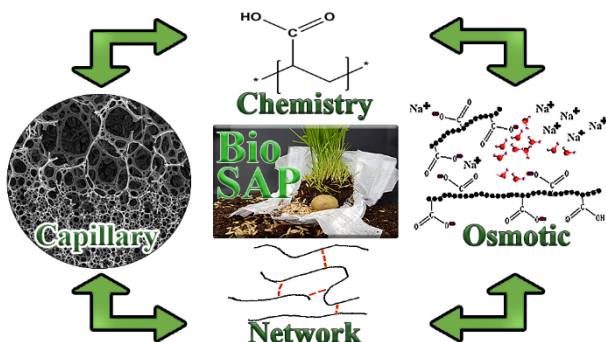
Uppskalningstester i form av extruderat WG material visade att den porösa strukturen hos de extruderade WG-materialen gav vattenupptag på 500 %. Uppskalningsmöjligheter för PPC absorbenter testades genom att funktionalisera potatisfruktsaft (PFJ), det vill säga PPC innan anrikning, och det visade sig att denna hade en vattenupptagningsförmåga på >10 g/g, vilket är jämförbart med det PPC-funktionaliserade materialet (>20 g/g). Dessa resultat banar väg för framtida optimering av produktionstekniker, vilka möjliggör för en hög produktionshastighet och massproduktion av hållbara proteinbaserade SAP: er.

Nyckelord proteiner, cirkularitet, superabsorbenter, hållbarhet, acylering, extrudering.

List of appended papers

Paper I

Advances in the Use of Protein-Based Materials: Toward Sustainable Naturally Sourced Absorbent Materials. Capezza, A. J.; Newson, W. R.; Olsson, R. T.; Hedenqvist, M. S. Johansson, E. *ACS Sustainable Chemistry and Engineering*, **2018**, 7(5), 4532-4547.



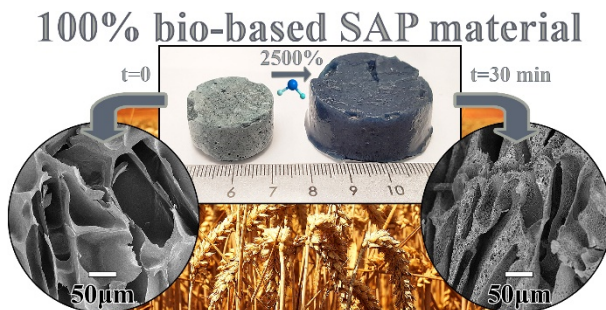
Paper II

A facile way of making inexpensive rigid and soft protein biofoams with rapid liquid absorption. Alander, B.; Capezza, A. J.; Wu, Q.; Johansson, E.; Olsson, R. T.; Hedenqvist, M. S. *Industrial Crops and Products*, **2018**, 119, 41-48.



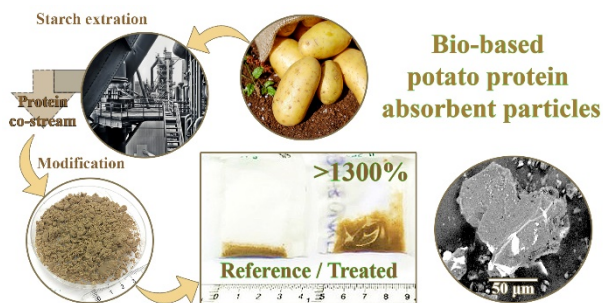
Paper III

Superabsorbent and Fully Biobased Protein Foams with a Natural Cross-Linker and Cellulose Nanofibers. Capezza, A. J.; Wu, Q.; Newson, W. R.; Olsson, R. T.; Espuche, E.; Johansson, E.; Hedenqvist, M. S. *ACS Omega*, 2019, 4 (19), 18257-18267.



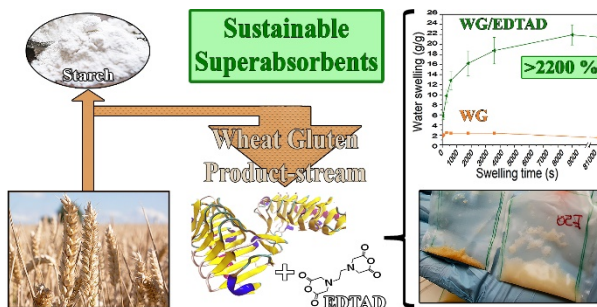
Paper IV

Novel Sustainable Superabsorbents: A One-Pot Method for Functionalization of Side-Stream Potato Proteins. Capezza, A. J.; Glad, D.; Ozeren, H.; Newson, W. R.; Olsson, R. T.; Johansson, E.; Hedenqvist, M.S. *ACS Sustainable Chemistry and Engineering*, 2019, 7 (21), 17845-17854.



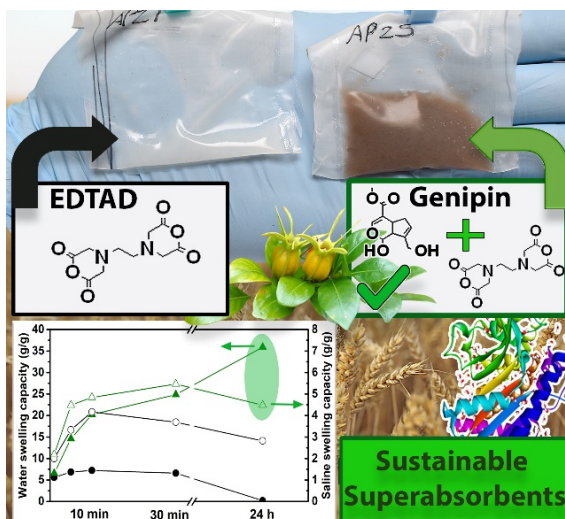
Paper V

Carboxylated wheat gluten proteins—a green solution for production of sustainable superabsorbent materials. Capezza, A. J.; Lundman, M.; Olsson, R. T.; Newson, W. R.; Hedenqvist, M. S.; Johansson, E. *ACS Biomacromolecules*, 2020, 21 (5), 1709–1719.



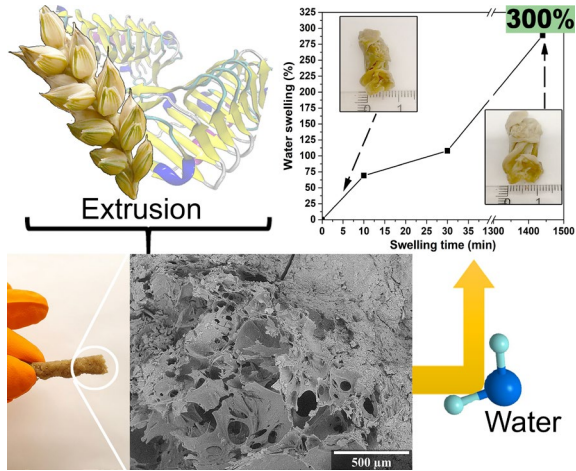
Paper VI

High Capacity Functionalized Protein Superabsorbents from an Agricultural Co-Product: A Cradle-to-Cradle Approach. Capezza, A., Cui, Y., Numata, K., Lundman, M., Newson, W., Olsson, R., Johansson, E., Hedenqvist, M. S. *Advanced Sustainable Systems*, 2020.



Paper VII

Extrusion of Porous Protein-Based Polymers and Their Liquid Absorption Characteristics. Capezza, A. J.; Robert, E.; Lundman, M.; Newson, W. R.; Johansson, E.; Hedenqvist, M. S.; Olsson, R. T. *Polymers*, 2020, 12 (2), 459.



Paper VIII (Manuscript)

Revalorization of a protein side-stream: an integrated industrial approach towards non-toxic biodegradable superabsorbents. Capezza, A., Muneer, F., Prade, T., Newson, W., Das, O., Lundman, M., Olsson, R., Hedenqvist, M., and Johansson, E. *Manuscript*.

The author's contributions to the appended papers:

Paper I: Performed all the planning, reference collection, and the manuscript writing.

Paper II: Participated in the planning, majority of the data analysis, and the manuscript writing.

Paper III: Performed, together with Qiong Wu, most of the experimental work (except SE-HPLC), all the data analysis, and the manuscript writing.

Paper IV: Performed all the planning, supervised all the experimental work, performed the majority of the data analysis (except XRD), and all the manuscript writing.

Paper V: Performed all the planning, the experimental work, the data analysis, and the manuscript writing.

Paper VI: Performed all the planning, the experimental work, the data analysis (except ^1H NMR), and the manuscript writing.

Paper VII: Performed all the planning, supervised the experimental work, performed the data analysis, and the manuscript writing.

Paper VIII (Manuscript): Performed all the planning, the majority of the experimental work, the data analysis (except the GWP), and the manuscript writing.

Other publications not included in the thesis:

An all-gluten biocomposite: Comparisons with carbon black and pine char composites. Das, O.; Hedenqvist, M. S.; Johansson, E.; Olsson, R. T.; Loho, T. A.; Capezza, A. J.; Raman, R. K.; Holder, S. *Composites Part A: Applied Science and Manufacturing*, **2019**, 120, 42-48.

A novel way of adhering PET onto protein (wheat gluten) plastics to impart water resistance. Das, O.; Loho, T. A., Capezza, A. J.; Lemrhari, I.; Hedenqvist, M. S. *Composites Part A: Applied Science and Manufacturing*, **2018**, 8(11), 388.

The development of fire and microbe resistant sustainable gluten plastics. Das, O.; Rasheed, F.; Kim, N. K.; Johansson, E.; Capezza, A. J.; Kalamkarov, A. L.; Hedenqvist, M. S. *Journal of Cleaner Production*, **2019**, 222, 163-173.

The Effect of Carbon Black on the Properties of Plasticised Wheat Gluten Biopolymer. Das, O.; Capezza, A.J.; Mårtensson, J.; Dong, Y.; Neisiany, R.E.; Pelcastre, L.; Jiang, L.; Xu, Q.; Olsson, R.T.; Hedenqvist, M.S. *Molecules*, **2020**, 25(10), 2279.

CONTENTS

1. PURPOSE OF THE STUDY	1
2. INTRODUCTION	2
2.1. Superabsorbent polymers	2
2.1.1. Superabsorbent polymers as core technology	5
2.2. Proteins	6
2.2.1. Protein structures and interactions	7
2.2.2. Proteins from agricultural co-products	8
2.2.2.1. <i>Wheat gluten proteins</i>	9
2.2.2.2. <i>Potato proteins</i>	9
2.3. Future technologies and solutions	10
2.3.1. Protein functionalization towards SAPs	10
2.3.2. Protein post-processing towards SAPs	12
2.3.3. Why protein from co-products?	13
3. EXPERIMENTAL	15
3.1. Materials and chemicals	15
3.2. Production of Superabsorbent Protein Porous Structures	16
3.2.1. Producing WG porous structures by sedimentation	16
3.2.2. Producing WG foams by lyophilization	18
3.2.2.1. <i>Lyophilized WG foams</i>	18
3.2.2.2. <i>Lyophilized WG/genipin foams</i>	18
3.2.2.3. <i>Lyophilized WG/CNF and WG/CNF/GEN foams</i>	19
3.2.3. Producing porous WG materials by extrusion	20

3.3. Production of Superabsorbent Protein Particles	22
3.3.1. Protein functionalization by “dry” acylation	22
3.3.2. Protein functionalization by “wet” acylation.....	24
3.3.2.1. <i>Acylation of WG</i>	24
3.3.2.2. <i>Acylation and genipin cross-linking of WG</i>	26
3.3.2.3. <i>Aqueous acylation of PPC</i>	28
3.4. Materials characterization	29
3.4.1. Free swelling capacity (FSC).....	29
3.4.2. Centrifuge retention capacity (CRC).....	30
3.4.3. Field-emission scanning electron microscopy (FE-SEM)	30
3.4.4. Size-exclusion high-performance liquid chromatography (SE- HPLC).....	31
3.4.5. Fourier-transform infrared spectroscopy (FTIR)	32
3.4.6. Thermal analysis and stability.....	33
3.4.7. Compression test.....	33
3.4.8. Particle charge density	34
3.4.9. ¹ H nuclear magnetic resonance (¹ H NMR).....	34
3.4.10. Time of flight mass spectroscopy (MALI-ToF-MS).....	35
3.4.11. Protein content analysis	35
3.4.12. Biodegradation and mould tests	35
4. RESULTS AND DISCUSSION	37
4.1. Production of WG porous structures	37
4.1.1. Liquid uptake of the WG-sedimented porous structures.....	37
4.1.2. Liquid uptake of the WG-lyophilized porous structures.....	39
4.1.3. Structural features of the WG-sedimented porous materials.....	41

4.1.4. Structural and chemical features of the WG-lyophilized porous structures	43
4.2. Production of solid particle protein-based superabsorbents .	49
4.2.1. PPC superabsorbents based on “dry”-acylation.....	49
4.2.1.1. <i>Liquid uptake</i>	49
4.2.1.2. <i>PPC functionalization</i>	50
4.2.1.3. <i>PPC particulate structure</i>	54
4.2.2. Solid particle protein superabsorbents based on “wet”-acylation	55
4.2.2.1. <i>WG/EDTAD particles</i>	55
4.2.2.2. <i>WG/EDTAD/genipin particles</i>	62
4.2.2.3. <i>PPC/EDTAD particles via aqueous acylation</i>	68
4.3. Upscaling production of porous WG structures	69
5. Conclusions	73
6. Future Work	76
7. Acknowledgments.....	77
8. References	79

Abbreviations

Superabsorbent polymers (SAPs)

Sodium neutralized polyacrylic acid (NaPAA)

Sodium hydroxide (NaOH)

Free swelling capacity (FSC)

Poly(ethylene terephthalate) (PET)

Absorption under load (AUL)

Room temperature (RT)

Relative humidity (RH)

Global Warming Potential (GWP)

Wheat gluten (WG)

Mild extracted wheat Gluten (WGm)

Potato protein concentrate (PPC)

Mild extracted potato protein (PPCm)

Potato fruit juice (PFJ)

Glutaraldehyde (GA)

Ethylenediaminetetraacetic dianhydride (EDTAD)

Ethylenediaminetetraacetic acid (EDTA)

Succinic anhydride (SA)

1,2,3,4-butanetetracarboxylic acid (BTCA)

Genipin (GEN)

Sodium bisulfite solution (NaHSO_3)

Ammonium sulfate ($(\text{NH}_4)_2\text{SO}_4$)

Cellulose nanofibers (CNF)

Sodium bicarbonate (NaHCO_3)

TEMPO-oxidized cellulose fibers (TEMPO)

Glycerol (Gly)

Size-Exclusion high-performance liquid chromatography (SE-HPLC)

Field emission scanning electron microscopy (FE-SEM)

Fourier-transformed infrared spectroscopy (FTIR)

Proton nuclear magnetic resonance (^1H NMR)

1. PURPOSE OF THE STUDY

Proteins obtained as co-products from agricultural industries are an under-utilized source of raw material that can have similar properties to petroleum-based plastics. The main purpose of the studies presented in this thesis was to develop plant protein-based materials with high liquid absorbency for applications in a sustainable personal hygiene industry. Readily available agricultural protein co-products, e.g., wheat gluten and potato protein, were utilized to add to value and also to provide environmentally-friendly materials that could be safely used in disposable single-use products, e.g., diapers. Agricultural proteins can be functionalized to mimic the chemical functions of synthetic industrial superabsorbents. The proteins can also be foamed to create porosity that could provide capillarity effects, which can contribute to rapid liquid absorption. The objective of the different studies described in this thesis was to process the proteins using harmless reagents and easily scalable protocols that could potentially be used for the personal hygiene industry in future. In particular, the protein modifications relied solely on chemical modification of the proteins, and recipes excluding any toxic cross-linkers/reagents in the process were devised. The modified proteins were swelled in water, saline solution, and defibrinated sheep blood, all liquids used as industry standards for testing in the personal hygiene industry. The resulting protein materials exhibited properties that are within the range of their synthetic counterparts, while still showing biodegradability. The experimental techniques used have the potential to be industrially-scalable, as some of the most common plastic processing methods were used, e.g. extrusion. The processes devised to offer environmentally friendly superabsorbent alternatives to the current non-sustainable materials used in the personal hygiene industry, representing a novel contribution to the scientific community. They also partly address some of the United Nations Sustainable Development Goals 2030, e.g., Responsible Consumption (by the users) and Novel Industry and Infrastructure (by providing new green alternatives).

2. INTRODUCTION

2.1. Superabsorbent polymers

Superabsorbent polymers (SAPs) are the core technology for many products where high liquid absorption and retention properties are required.^[1-3] SAPs are extensively used in care and personal hygiene products, representing up to 40 % of the dry weight of such products.^[2,3] SAPs are also used in other application areas e.g. pharmaceuticals, agriculture, and active hydrogels.^[3-9] SAPs consist of soluble polymeric carbon chains with charged/polar side-groups such as hydroxyl, carboxylic acid, and amides, forming polyelectrolytes.^[1, 2, 10] A common example of SAPs encountered in commercial products is sodium neutralized poly(acrylic acid) (NaPAA).^[11] To prevent the water-soluble polymer from dissolving, a 3D network is formed by covalent cross-links, and the cross-linking degree has been reported as low as 8×10^{-4} crosslinks/mol.^[1, 10, 11] The charged nature of the polymer, coupled with the low degree of cross-linking, provides the polymer with water absorption values of 10-100 g water/g dry SAP and 5-50 g in ionic liquids (typically 0.15M NaCl)/g dry SAP.^[3, 12] The NaPAA structure in dry and wet state is shown in Figure 1.

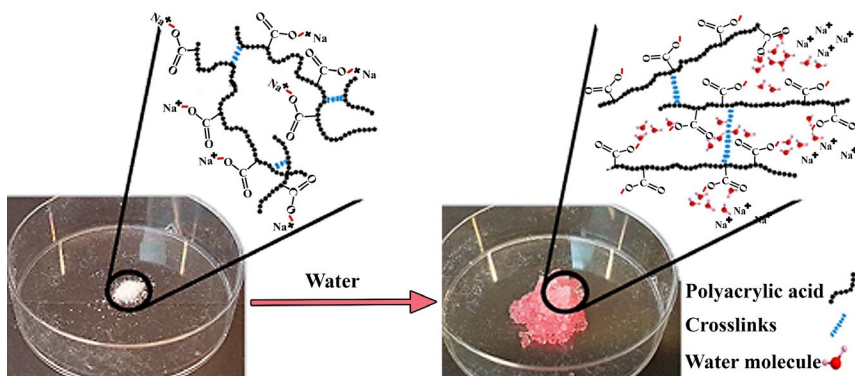


Figure 1. Commercial superabsorbent polymer (SAP) particles in (left) the dry state and (right) the wet state. A red dye was used in the water for clarity. Adapted from Paper I.^[3]

The swelling properties of SAP materials mainly derive from the high osmotic and charge repulsion effects occurring when the materials are in contact with water.^[3, 13-17] To maximize the osmotic effects, the charged group in SAP is neutralized after polymerization, typically by adding sodium hydroxide (NaOH).^[3] When the SAP is placed in water, an initial chemical potential difference between the surface of the SAP chain (C_g) and the liquid (C_s) is generated, leading to development of the osmotic effects (Π_{ion} , in atm).^[18, 19] Combinations of different counterions and neutralization degree are often used in the industry to influence the absorption kinetics of the material.^[20-24] The osmotic pressure that develops in the material upon liquid absorption can be explained by the Van't Hof Law:^[3, 19]

$$\Delta\Pi_{ion} = RT (\sum C_g - \sum C_s) \quad (\text{Equation 1})$$

where R is the gas constant ($\text{m}^3\cdot\text{atm}/\text{K}\cdot\text{mol}$).

According to the Van't Hof Law, the greater the difference between the total ionic species in the solution and the SAP, the higher the osmotic effects. Thus, the swelling degree of SAPs can decrease up to 10-fold times when ionic liquids such as saline or urine solutions are used instead of pure water.^[3]

Once the liquid has started to diffuse into the SAP chains, the counterions are gradually diluted in the liquid, thus exposing the charged groups in the polymer and generating network expansion due to electrostatic repulsions (Figure 1).^[25-27] Accordingly, highly charged polymeric chains, e.g., polyelectrolytes, are preferred in fabrication of SAP materials. During swelling, expansion/deformation of the polymeric network continues and the polymer chain relaxation will depend on the cross-linking degree of the material.^[14] Such cross-linking degree follows rubber deformation theory, which states that a low cross-linking degree provides less polymer network restriction, thereby allowing greater expansion of the SAP.^[1, 2] The swelling process in SAP proceeds until equilibrium is reached. A more detailed description of the swelling process is provided by the Flory-Huggins equation,

which includes the mixing and rubber network parameters.^[1, 2, 25-27] Thus, the osmotic effects expressed in Equation 1 can be expanded to:

$$v_a \Pi = kT \left[\frac{\phi}{Nb} \left(\frac{1}{2} - \left(\frac{\phi_o}{\phi} \right)^{2/3} \right) - (\phi + \chi \phi^2 + Ln(1 - \phi)) \right] \text{ (Equation 2)}$$

where v_a represents the molecular volume (m^3 / mol), Nb the chain length between crosslinks, χ the Flory-Huggins interaction parameter, and ϕ_o and ϕ the polymer volume fraction in the dry and swollen state, respectively.

From the polymer chemistry perspective, besides the variations in cross-linking density, neutralization degree, and chain length that allow tuning of SAP swelling properties, parameters such as group functionality, functionality equivalent content, cross-linking type/length, among others, are also used industrially to influence the SAP swelling kinetics.^[28] Other approaches to adjust the swelling kinetics rely on physical modifications of the SAP during post-processing. For instance, induced porosity in the SAP (either open or closed pores) is used to facilitate liquid diffusion within the SAP particles, thereby providing fast -initial absorption compared with solid SAP particles.^[29-33] The effect is provided by capillarity-driven forces, which have been shown to be the main mechanism governing volumetric flow of the liquid within the porous SAP structure used in some commercial personal hygiene products such as sanitary pads.^[3, 9] The capillarity-driven effect, related to the surface tension of the liquid/material, is described by the Laplace Law:^[30, 34, 35]

$$\Delta p = \rho g h = 2 \sigma / R \text{ (Equation 3)}$$

where Δp is the differential capillarity pressure (Pa), ρ the density of the fluid (kg/m^3), g gravity (m/s^2), R and h the radius and height of the capillary (or pore, in m), and σ the surface tension (N/m).

2.1.1. Superabsorbent polymers as core technology

Many products rely on SAP as the core technology for fulfilling their tasks. For example, SAP represents the main technological improvement in many products, such as making baby diapers and sanitary pads thinner and more efficient.^[1, 2, 36] Disposable diapers account for up to 10% of the SAP market, but are also the most demanding application among the SAP-related products.^[37, 38] In diapers, SAP free swelling capacity (FSC) of 50 g/g and absorption under load (AUL) (simulating the user's weight on the product) of 30 g/g are required.^[3] In other SAP-related application areas, a material with water and saline swelling capacities above 10 g/g and 2 g/g, respectively, is considered a SAP.^[15, 39, 40] Figure 2 shows the main parts of a baby diaper as an illustrative example.

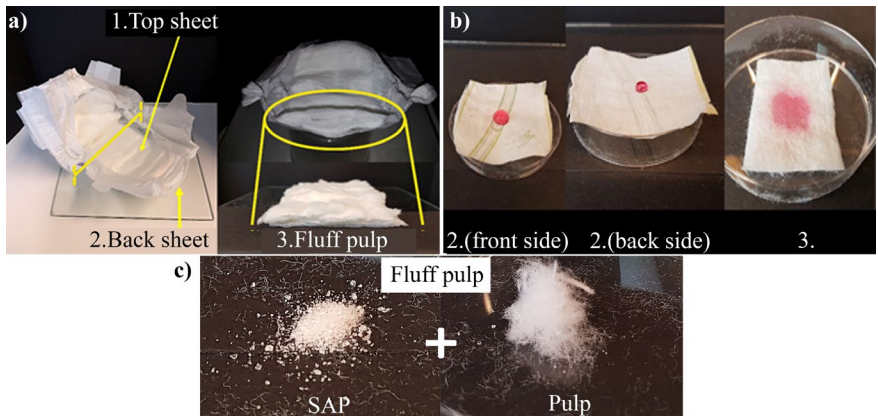


Figure 2. (a) A commercial baby diaper and its different parts. (b) The back sheet (2) and top of the fluff pulp (3) exposed to a water droplet with a red dye to illustrate their liquid interaction properties. (c) Components of the fluff pulp.

A disposable diaper is made up from three main sections: i) a non-woven polypropylene-based top sheet, ii) a polyethylene-based back sheet, and iii) and a fluff pulp pad (Figure 2a). The non-woven polypropylene sheet allows transport of body fluids from the user to the inner core, and thus no swelling occurs at this hydrophobic layer.^[1, 2] The fluff pulp pad is located at the core

of the diaper's cross-section and consists of non-woven cellulose fibers with SAP particles homogenously mixed into the fiber' matrix (Figure 2c).^[38] The cellulose fibers allow the fluids to spread throughout the entire fluff pulp pad, maximizing SAP absorption and avoiding gel-blocking effects.^[1-3] The hydrophobic polyethylene/ polypropylene back sheet film stops the liquid from leaving the product (Figure 2b, point 2).^[41]

Work is underway to decrease the amount of cellulose pulp in disposable diapers (or any other incontinence product), through the fabrication of thinner products, to decrease their environmental impact. The environmental impact of a disposable diaper was decreased by 55 % from 1987 to 2011, by reducing the amount of cellulose pulp.^[42] The negative impact reported for the cellulose fraction is due to toxic components released during pulp refining. The SAP still accounts for 25 % of the reported Global Warming Potential (GWP) of a single diaper from the equivalent mass of CO₂ released per unit (based on 100-year calculations).^[43] Many innovations have relied on replacement of the polyethylene and polypropylene components with bio-based polymers to decrease the environmental impact of disposable products.^[3, 38, 44] However, the SAP has not been replaced in any personal hygiene product so far. This, coupled with the exponential increase in the SAP market and the related emerging applications, show that replacement of the current petroleum-based SAP with a sustainable alternative would enable production of safe greener products.^[3]

2.2. Proteins

Proteins are considered one of the most important naturally-occurring macromolecules, having fundamental functions in living organisms, such as transportation, catalysis, and formation/regulation of structural tissues (e.g., body organs).^[45-48] Proteins can also be involved in the formation of complex structures to impart e.g., mechanical strength and high flexibility to spider silk, forming materials stronger than steel.^[49, 50] Compared with other naturally-occurring polymers, proteins have the ability to be hydrolyzed and self-

polymerized into nano-assemblies, forming nanofibrils that could be the base for future food items and materials.^[51, 52] In the material sciences field, plant proteins have been used to produce bio-based materials which replicate the properties of viscoelastic petroleum-based plastics, due to ability of proteins, e.g., wheat proteins, to form network.^[53-61]

2.2.1. Protein structures and interactions

A protein chain (polypeptide) is made up of amino acid residues (monomers), which are linked by peptide bonds (Figure 3).^[46, 48, 62] The amino acid residues differ depending on the functional group “R” attached to the α -carbon, and approximately 20 protein-building amino acid residues are known.^[3, 63, 64] The composition and order of residues in the polypeptide chain is known as the primary structure of proteins.^[65] Due to the functional nature of the different amino acids, interactions (hydrogen bonds, hydrophobic interactions, etc.) can be established within the individual protein chains, which causes the chains to fold and form structures such as α -helices and β -sheets (Figure 3).^[3] This is known as the secondary structure of proteins. For energy minimization, covalent and non-covalent intra-protein interactions can be formed within the polypeptide, giving rise to the development of the polypeptide 3D-structure known as tertiary structure.^[3, 62, 66] Several of the physical and chemical properties of proteins are a macroscopic expression of their tertiary structure. The individual 3D-structures in proteins can also interact with each other by inter-protein interactions to form the largest protein assembly complex, known as quaternary structure.^[3, 63, 64]

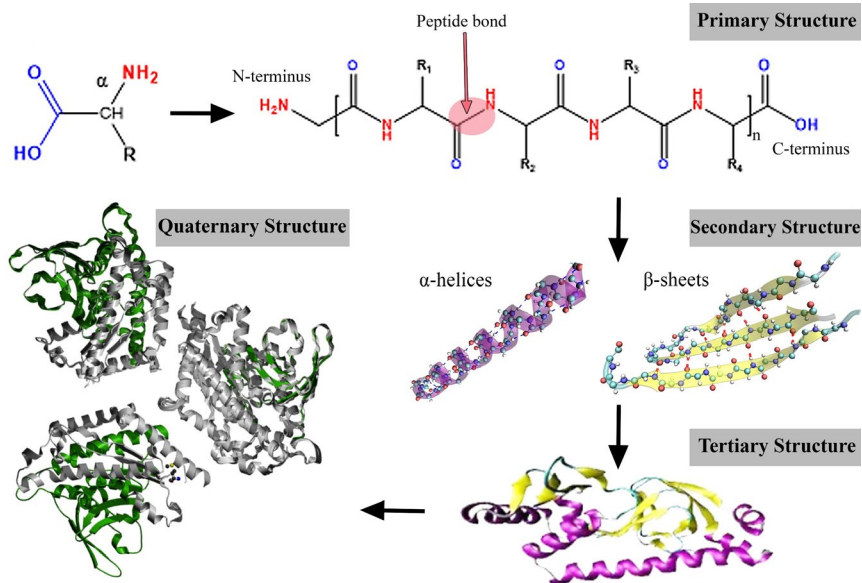


Figure 3. Polypeptide and a representation of the hierarchical protein structure.

Related to chemical features of the polypeptide chain, the carbonyl group ($\text{C}=\text{O}$) and the $-\text{C}-\text{N}$ bond, which has physical features resembling a double bond, imparts rigidity to the protein chain.^[46, 67] Thus, the conformational state energy of protein is typically greater than that of other natural-occurring macromolecules, e.g., polysaccharides.^[46, 67] To tackle protein rigidity issues in the design of bio-based materials, plasticizers (e.g., glycerol) are commonly added to make their processing easier while maintaining their mechanical properties.^[57-59]

2.2.2. Proteins from agricultural co-products

Several agricultural industries are currently producing large amounts of proteins from different crops, which are obtained as a co-product e.g., from the starch or bioethanol industries.^[3] For instance, in 2018 around 3.7 million tons of potato starch were produced,^[68] representing 10 million m^3 of potato fruit juice (as a by-product) and around 200 000 tons of potato protein.^[69, 70] Although such proteins can be sold as animal feed or as food additives,

industries are constantly searching for innovations where these protein co-products could be used.^[3]

2.2.2.1. Wheat gluten proteins

Wheat (*Triticum aestivum*) is the largest crop cultivated worldwide and a more important food grain source for humans than any other commercial crop. According to the Food and Agricultural Organization of the United Nations (FAO), global wheat production was 734 million tons in 2018.^[71] The total protein content of wheat is 11-20 wt.%, and it consists of non-gluten and gluten proteins (75-85 wt.%).^[45, 72] The wheat gluten (WG) sub-fraction is further divided into gliadins (30-60 kDa) and glutenins (30-3000 kDa). WG can be obtained as a concentrate after starch extraction from wheat (as a co-product), with current global WG production estimated to be ~1 million tons.^[45, 60, 61, 65, 72] WG is known to show viscoelastic properties, which are responsible for mechanical integrity in breadmaking.^[73] Such viscoelastic properties make WG a suitable alternative for some applications where fossil-based polymers are used. WG-based materials have been fabricated using traditional polymer processing techniques, e.g., extrusion, compression molding, and foaming.^[45, 74-78]

2.2.2.2. Potato proteins

Potato is one of the main tuber crops cultivated worldwide, with around 368 million tons harvested globally in 2018.^[70, 71, 79-81] Potato protein sub-fractions consist of patatin (a glycoprotein, 40 kDa), protease inhibitors, and a complex of mixed proteins. Patatin, a water-soluble protein, represents the largest protein fraction (40 %) of the total potato protein content. Potato protein can be obtained as a concentrate (PPC) co-product of starch extraction from potato tubers.^[70, 79-81] After starch extraction, a juice rich in potato protein (PFJ) and containing 20-60% of the total dry potato protein is obtained.^[82] The proteins contained in PFJ are precipitated using harsh acidic and temperature conditions resulting in PPC.^[82] The harsh processing conditions lead to extensive protein aggregation, loss of vital properties, co-

precipitation of toxic glycoalkaloids, and protein insolubility.^[69, 83, 84] Thus, the added value of PPC is low, and so far only low-quality fertilizer or animal feed products can be produced from PPC. Novel opportunities for the development of bio-based materials using PPC have been reported, where compression molding techniques have been used.^[53, 55, 59]

2.3. Future technologies and solutions

In general, proteins as a source for the development of bio-based material have not been extensively studied compared with polysaccharides.^[3] The heterogeneity and processing difficulties represent a challenge to the use of proteins in the plastics industry. However, it has been demonstrated that protein co-products, e.g., WG, PPC, and rapeseed proteins, provide extensive chemical functionality, and their properties can be fine-tuned for producing antimicrobial, electrically conductive, flame-resistant and liquid-absorbent materials.^[85-93] Liquid absorption properties of protein co-products are reported to be within the same range as those of synthetic SAPs, making them a promising candidate for production of bio-based SAPs.^[94-96]

2.3.1. Protein functionalization towards SAPs

The heterogenous protein chemical structure represents a challenge compared with polysaccharides (which mainly have hydroxyl groups unless treated), especially in chemical reaction and/or physical modification of the polypeptide chains.^[3] Several studies have reported grafting synthetic acrylic acid monomers onto different proteins, and subsequent polymerization of the acrylic monomer to impart SAP properties.^[97-101] Although polymerization of SAP onto protein provides superabsorbance properties, synthesis of hybrid material does not fulfil the environmental criteria, as it does not fully replace the non-sustainable petroleum-based monomer in the recipe.^[102]

Mimicking the functionality of synthetic SAP by chemical acylation of plant proteins has been identified as the most promising way to produce protein-based SAPs.^[3] Acylation of proteins consists of condensation of acyl

groups (-COR) to the protein by reacting to the primary amine (-NH₂) groups within the proteins (grey area in Figure 4).^[39, 40] Such acylation leads to formation of a covalent amide bond and thereby pendant charged carboxylic acid moieties, as shown in Figure 4.^[39, 40] Soy and fish protein have been successfully acylated using ethylenediaminetetraacetic dianhydride (EDTAD), which provides three charged carboxylated groups (-COO⁻) per EDTAD molecule condensed.^[39, 40, 103-108] The carboxylated groups originate from ring-opening of the highly reactive furodianone group in EDTAD.^[39, 40] EDTAD-functionalization of proteins is reported to result in swelling capacity of 30-540 and 10-40 g/g in pure water and saline solution, respectively.^[3] A schematic diagram of EDTAD condensation on the lysine residue of protein is shown in Figure 4.

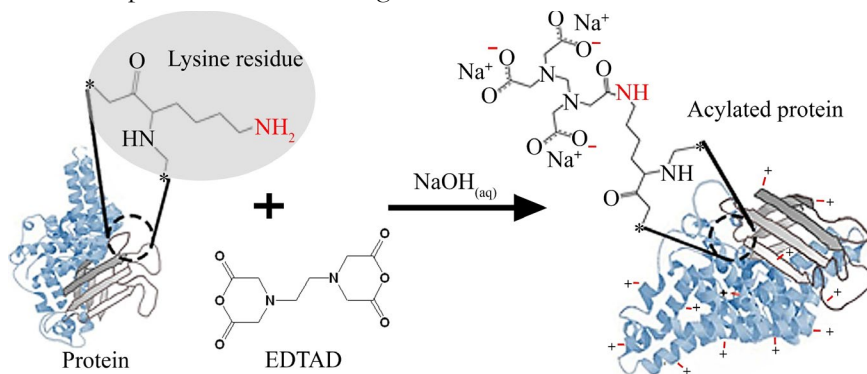


Figure 4. Schematic diagram of the EDTAD condensation reaction with the lysine residue of protein to produce bio-based superabsorbent polymers (SAP). Adapted from Paper I.^[3]

To expose the functional groups in the protein, which results in more efficient chemical treatment, thermal (60°C for 30 min) and alkaline denaturation (pH>11) of the protein is typically performed.^[3] The acylation reaction of proteins is favored by using dilute aqueous solutions (2-4 wt.%) and pH above the pK_a of lysine (10.4) to increase its reactivity.^[39, 40] Other acylation reagents, such as succinic anhydride (SA) and citric acid (CA), have been also used to functionalize proteins.^[109-111] However, EDTAD is preferred, as the reaction produces easily washable non-toxic

ethylenediaminetetraacetic acid (EDTA) as a by-product, while the EDTAD also provides higher functionalization efficiency (producing three charged groups) than the other acylation agents.^[3]

2.3.2. Protein post-processing towards SAPs

Providing proteins with a stable network ensures minimal leakage of the polymer from the SAP products during swelling, as well as imparting higher strength to the gel structure.^[29, 86] The gel network is typically achieved by cross-linking the protein. Aldehydes are the most commonly used cross-linkers for protein-based materials, including protein-based SAP. Glutaraldehyde (GA) is known in particular to effectively cross-link proteins at a fast reticulation rate, using lysine moieties in the protein as the main reactive site.^[112-115] However, the typical cross-linking agents used in proteins are considered toxic and not environmentally friendly, which can be a bottleneck in development of bio-based SAP products for personal hygiene uses.^[3]

Post-processing of protein-based SAP also involves modification of product morphology, e.g., by generating interconnected channels promoting capillary uptake (foam structures) or by increasing the surface area (finely divided structures).^[29, 31, 93] It has been demonstrated that swelling equilibrium, absorption rate, and liquid diffusion can be tuned by solely generating foam-like structures (without involving any chemical processes), and modification of their pore size and pore size distribution.^[3] Protein-based foams for SAP-related applications, e.g., pH-sensitive hydrogels, blood and plasma absorption, etc., have been produced in this way.^[3] Proteins such as WG combine high viscoelastic properties with liquid absorption, which is critical for the development of stable foam structures. WG foams have water swelling capacity of ~ 32 g/g and mechanical properties that resemble synthetic SAP materials.^[29, 93, 112]

2.3.3. Why protein from co-products?

Recent studies have focused on production of bio-based materials from a holistic perspective, taking a cradle-to-cradle design approach.^[116] For bio-based SAP to have future prospects, factors from the raw material extraction/production/consumer chain, etc. have to be considered, including the source of the raw material, reagents used, impact of product use, disposal of the product, and other circular bio-economy factors.^[116]

Proteins obtained as co-products, e.g., from starch extraction and bioethanol production, make a sustainable, inexpensive, and reliable feedstock.^[102, 116] The estimated cost of WG and PPC is ~1.2 and 1 EUR/kg, respectively, which is comparable to the price of synthetic SAP (1.50 EUR/kg).^[79, 86, 116] There is currently no commercial production of protein-based SAPs, while commercial production of cellulose-based SAPs is also limited as the cellulose is mostly extracted from the forest industry. Hence, the SAP business based on cellulose is impaired by the need to harvest more forest hectares, adding to deforestation. In Sweden, around 10 000 tons of PPC and 20 000 tons of WG protein co-streams are produced today. These protein concentrates can be available for future production of novel protein-based SAPs, without significantly influencing the food market.^[79, 86, 116] The wide variation in different protein co-product sources presents a challenge in materials manufacture. However, the variation within the protein co-products also opens up valuable opportunities to tune the properties and reaction mechanisms of the proteins, generating tailored materials with different swelling properties.^[3] In addition, the use of processes for the protein modification that do not involve toxic chemicals can lead to the development of a safer disposable product.

Regarding the possibility of manufacturing SAP from bio-based monomers, similar to the manufacture of polylactic acid (PLA), life cycle analysis has shown that utilization of e.g., WG as a co-product from the wheat starch industry results in less environmental impact than PLA.^[117] Moreover, SAP synthesized from bio-based monomers (or even PLA) needs to be

polymerized to produce SAPs, whereas protein-based SAPs rely on a naturally-formed polymer, so no energy is needed for synthesis of the material. Production of protein-based SAP should rely on a commonly used polymer processing technique, e.g., extrusion, so that it does not require major industrial changes and can make synergistic contributions to the cradle-to-cradle model.^[118] Proteins have shown the capacity to be successfully processed using e.g., extrusion, implying that the cost to industries of adapting/optimizing their current processes towards manufacturing of protein-based SAPs can be low.^[118]

3. EXPERIMENTAL

3.1. Materials and chemicals

Wheat gluten concentrate (WG) was provided by Lantmännen Reppe AB, Sweden. The protein content was 86.3 ± 0.3 % (Dumas method, NMKL 6:2003, U.S.A., N x 6.25). Potato protein concentrate (PPC) was provided by Lyckeby Starch AB, Sweden. The PPC protein content was 82 ± 2 % (determined as described in section 3.3.11). Both WG and PPC were used as-received and always stored in a silica-gel desiccator.

To investigate possible effects of the industrial production process for WG and PPC, which has been shown to cause some protein aggregation, WG and PPC were also extracted in-house using mild extraction procedures (WGm and PPCm, respectively).^[60] Extraction of WGm involved of wrapping 20-30 g of wheat flour in a piece of fine cloth and thoroughly washing with running water, thus removing the starch. The washing continued until a yellow sticky dough was obtained. Thereafter, the concentrated WGm was frozen at -80 °C and lyophilized for 72 h.

Extraction of PPCm involved ammonium sulphate precipitation.^[81] In brief, commercial potato tubers were washed with water, peeled and dipped in 2 wt.% sodium disulphide solution (NaHSO_3) to avoid excessive enzymatic browning. The potatoes were then juiced in an Angelia 5500 twin screw press (Angel Co. Ltd., South Korea), and the potato juice was allowed to settle for 15 min at room temperature (RT). The juice was centrifuged at 3000 RCF for 15 min at 10 °C and the supernatant was vacuum-filtered using a 30-50 μm filter paper. The pH of the potato fruit juice (PFJ) was measured using a pH-meter (Mettler-Toledo, Switzerland). Ammonium sulfate ($(\text{NH}_4)_2\text{SO}_4$) was added to the PFJ to 60 % of the saturation limit of PFJ, i.e., 542 g/L at 25 °C. The pH of the suspension was monitored and corrected to 5.7 by adding 0.5 M H_2SO_4 . The solution was stirred at 4 °C for 1.5 h and then centrifuged at 3000 RCF for 30 min at 4 °C. The pellet was re-suspended in MilliQ water (MQw) and dialyzed using a 10-30 kDa cut-off dialysis membrane. Thereafter,

the cleaned PPCm was frozen at -80 °C and lyophilized for 72 h. The protein content of both WGm and PPCm was calculated using the Dumas method as described in section 3.3.11, and found to be $85.5 \pm 0.6 \%$ and $94 \pm 0.5 \%$, respectively.

Ethylenediaminetetraacetic dianhydride (EDTAD, >98%), ethylenediaminetetraacetic acid (EDTA, $\geq 99\%$), succinic anhydride (SA, $\geq 99\%$), 1,2,3,4-butanetetracarboxylic acid (BTCA, 99%), and citric acid (CA, $\geq 99.5\%$) were all purchased from Sigma-Aldrich, Sweden. Glutaraldehyde grade II 25 vol.% (GA) was purchased from Sigma Aldrich. Glycerol HPLC-grade (99%) was obtained from Fisher Scientific, Sweden. Genipin HPLC grade (GEN, >98%) was purchased from Zhixin Biotechnology, China. Sodium hydroxide (NaOH, >98%), sodium disulphide solution (NaHSO_3 , >99%), ammonium sulphate ($(\text{NH}_4)_2\text{SO}_4$, >99%), and sodium bicarbonate (NaHCO_3 , >99.7%) were purchased from Sigma Aldrich. Cellulose nanofibers (CNFs) were purchased as a commercial type of Nata de Coco before extraction and were used as-received. For this product, CNFs with specific surface area $160 \text{ m}^2/\text{g}$, average length 2-3 μm , and diameter <10 nm have been reported.^[119] The extracted CNF was available as a 0.4 wt.% aqueous dispersion at neutral pH. TEMPO-mediated oxidized cellulose fibers (TEMPO) were used as-received, prepared as previously described.^[120] The TEMPO had an estimated charge of $10 \mu\text{eq}/\text{g}$, and the fibers obtained had diameter $2.4 \pm 0.7 \text{ nm}$.

3.2. Production of Superabsorbent Protein Porous Structures

3.2.1. Producing WG porous structures by sedimentation

Sedimented porous WG structures were prepared by mixing the as-received WG powder in 100 mL MQw containing pre-mixed glutaraldehyde (GA). The different recipes used are summarized in Table 1. For sample preparation, the mixture was stirred using a Ultraturrax Yellow Line Di 25 basic homogenizer equipped with a S25N-18G dispersion tool (IKA, Sweden)

for 2 min at 13000 rpm (Figure 5, step 1). The mixture was then decanted into cylindrical (40 mm diameter and 25 mm height) or cubic (20 x 20 mm) PET molds with pre-perforated holes at the bottom of the mold to allow water drainage (Figure 5, step 2). The mixture was evenly distributed in the molds and the samples were allowed to dry at room temperature for 24 h. The semi-dry samples were carefully removed from the PET molds and allowed to dry at ambient conditions for at least 1 week (Figure 5, step 3). The cubic samples were only used for the liquid absorption tests and the cylindrical samples for mechanical characterization.

Table 1. Composition of the mixtures used for production of wheat gluten (WG) porous structures by sedimentation.^a GA = glutaraldehyde.

Sample	WG (g)	GA (g)	Glycerol (g)	TEMPO ^{nc} (g)
WG/Reference	20	0.5	0	0
WG/high-WG	30	0.5	0	0
WG/Gly	20	0.5	6	0
WG/TEMPO	20	0.5	0	0.2
WG/TEMPO/Gly	20	0.5	6	0.2

^a100 mL Milli-Q water was used in the recipes. For the TEMPO cellulose samples, less water was added to compensate for the water in the TEMPO cellulose gel.

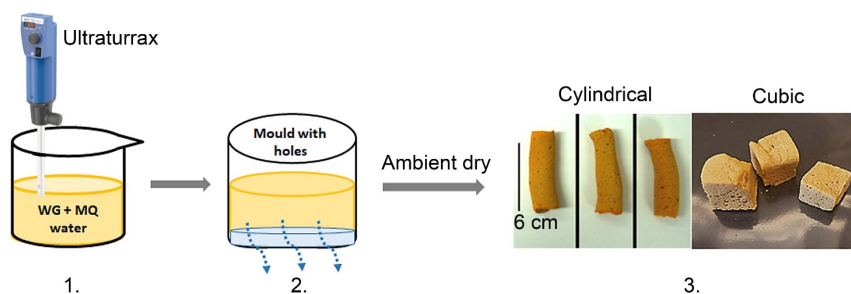


Figure 5. Preparation procedure for production of porous wheat gluten (WG) structures by sedimentation.

The amount of GA used (0.5 g GA/20 g WG = 2.5 wt.%) was based on optimization tests where mixtures containing 0.5, 1, 2.5, 5, and 10 wt.% GA (related to WG content) were prepared.^[112] The selection was based on the mixture that gave the best properties (less shrinkage and tackiness). The

glycerol content was based on previous studies, where 30 wt.% glycerol was used in production of flexible WG foams.^[92] Likewise, the TEMPO content used (1 wt.%) was based on previous work on freeze-dried WG using 1 wt.% bacterial cellulose fibers.^[74] To evaluate the influence on mixture properties and stability of the WG content, one sample was prepared by adding additional WG to the mixture (Table 1).

3.2.2. Producing WG foams by lyophilization

3.2.2.1. Lyophilized WG foams

The WG foams were prepared by lyophilization as previously described.^[89] In brief, 20 g of the as-received WG powder was gradually added to a beaker containing 100 mL of MQw (pre-adjusted to pH 11) under constant stirring. The pH of the mixture was monitored and adjusted to pH 11 by adding 1M NaOH. The mixing continued until more or less stable pH 11 was reached, after ~10 min. Additional MQw was added to the mixture to give a total volume of 120 mL (Figure 6, step 1). To achieve protein denaturation, expose the functional groups, and promote disulphide cross-linking, the WG dispersion was heated in a silicone oil bath to 90 °C for 30 min, with simultaneous homogenization using an ultraturrax at 9500 rpm (Figure 6, step 2), producing a foam. When the foaming process was completed, which resulted in a volume increase of ca. 300%, the mixture was removed from the bath and left at room temperature to cool the suspension. The mixture was poured into cuboid silicone molds with dimensions 10 × 10 × 11 mm (Figure 6, step 4), stored at -25 °C for 12 h, and subsequently lyophilized for 48 h. This sample is referred to as 'WG'.

3.2.2.2. Lyophilized WG/genipin foams

Lyophilized WG/GEN foams were prepared following the procedure described in section 3.2.2.1. However, when the WG foamed suspension was removed from the silicone oil bath (90 °C), the mixture was cooled down to 40 °C and 200 mg of genipin powder (GEN; 1 wt.%) were added while

keeping the mixture under continuous mixing for 2 h (Figure 6, step 3). During the reaction time (2 h at 40 °C), a gradual change in the mixture color from yellow to green was observed. Thereafter, the mixture was cooled to room temperature, poured into cuboid molds, frozen at -25 °C for 12 h, and lyophilized as for the WG foams. This sample is referred to as ‘WG/GEN’.

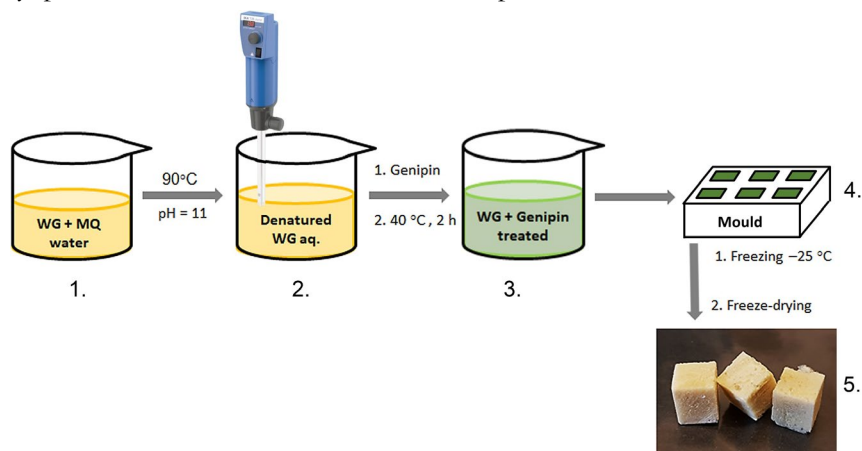


Figure 6. Preparation procedure for production of lyophilized wheat gluten (WG) foams.

3.2.2.3. Lyophilized WG/CNF and WG/CNF/GEN foams

As-received CNFs, extracted from bacterial cellulose cubes, were used to study the influence of the nanofiller on the mechanical properties of the WG foams. The WG/CNF foam was prepared as described in section 3.2.2.1. The extracted CNFs were added to the MQw before WG addition (Figure 6, step 1), until a concentration of 1 wt.% CNF (based on the WG content) was reached, which required 200 mg CNFs. Sample preparation then proceeded in the same way as for the WG foams (section 3.2.2.1.). This foam is referred to as ‘WG/CNF’.

To evaluate the possible effects of combining GEN and CNFs on the WG foams, 200 mg of GEN were added to the sample prepared as described above (containing 200 mg of extracted CNFs) when the mixture had been

cooled to 40 °C. The mixture was prepared as in section 3.2.2.2. (2 h reaction time at 40 °C) and lyophilized as for the WG foam. This foam is referred as to 'WG/CNF/GEN'.

3.2.3. Producing porous WG materials by extrusion

For preparation of the mixture, 100 g of the as-received WG powder were gradually added to 100 mL MQw under constant magnetic stirring. The MQw was pre-adjusted to pH 11 (using 1 M NaOH) and the pH of the mixture was monitored using pH paper strips and corrected to pH 11. The mass ratio was selected after optimization tests, which resulted in 1:1 WG:water being the most cohesive while providing the best extrudates. Manual mixing was used once the mixture became too viscous for magnetic stirring (after addition of around 30 g of WG). The total mixing time was ~15 min.

For the extrusion, the WG mixture (with consistency resembling dough for breadmaking) was immediately transferred to an Axon BX18 extruder (Axon AB, Sweden) (Figure 7, step 1). The extruder, equipped with four heating zones at the barrel and one at the die, was preheated to 20 - 50 - 60 - 70 - 80 °C (Low Temperature profile, LT), and 20 - 90 - 100 - 110 - 120 °C (High Temperature profile, HT) (Figure 7, step 2). A circular die with a 6 mm diameter and a screw speed of 20 rpm were always used. It should be noted that the extrusions were generally discontinuous, due to built-up of pressure in the extruder die. Once extruded, the WG strands were placed in a forced-air oven at 40 °C for 24 h (Figure 7, step 3). The WG extruded materials were kept inside silica-containing desiccators for 1 week prior to testing. The pore structure of the extruded material was compared with that of the lyophilized WG mixture before extrusion. The mixture was placed in cuboid molds (10 x 10 x 11 cm³), frozen at -25 °C for 24 h, and lyophilized for 48 h. This sample is referred to as 'WG(f)'.

To evaluate the effect of adding plasticizer on the WG mixture/extrudates, 5 wt.% of glycerol (related to WG content) was added to

the MQw (pre-adjusted pH 11) prior to gluten addition. Sample preparation and extrusion followed the steps described above and these samples are referred to as ‘WG 5G LT’ and ‘WG 5G HT’. Sodium bicarbonate (NaHCO_3), was also used to evaluate the effect of a physical foaming agent in the recipe. The WG mixture preparation was the same as described above, but after mixing the WG with water (pre-adjusted to pH 11), 5 g of $\text{NaHCO}_3/100$ g WG were added, as shown in Figure 7 (step 1). The mixture was thoroughly mixed manually before extrusion. These samples are referred to as ‘WG 5S LT’ and ‘WG 5S HT’.

An additional sample was prepared by adding both glycerol and NaHCO_3 to the WG recipe. After the mixing the WG with water (pre-adjusted to pH 11 and containing 5 wt.% of glycerol relative to the gluten content), 5 g of $\text{NaHCO}_3/100$ g WG were added to the mixture. The mixture was thoroughly mixed and thereafter extruded as described above. These extrudates are referred to as ‘WG 5G5S LT’ and ‘WG 5G5S HT’. The different samples prepared using the extrusion protocol and their respective formulations are described in Table 2.

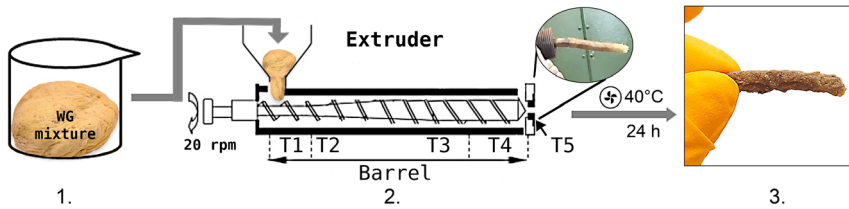


Figure 7. Preparation procedure for production of porous wheat gluten (WG) materials by extrusion.

Table 2. Sample formulations and extrusion parameters used for production of porous wheat gluten (WG) materials by extrusion. Adapted from Paper VII.

Sample name	WG (wt%)	Water (wt%)	Glycerol (wt%)	NaHCO ₃ (g/100g WG)
WG LT	50	50		
WG HT	50	50		
WG 5G LT	50	45	5	
WG 5G HT	50	45	5	
WG 5S LT	50	50		5
WG 5S HT	50	50		5
WG 5G5S LT	50	45	5	5
WG 5G5S HT	50	45	5	5

¹ LT: low temperature: 20 - 50 - 60 - 70 - 80 °C (± 10 °C), HT: high temperature: 20 - 90 - 100 - 110 - 120 °C (± 10 °C). All samples were extruded at a screw speed of 20 rpm. The production rate was 6.6 g/min (0.4 kg/h) and 3.24 g/min (0.2 kg/h) for LT and HT, respectively.

3.3. Production of Superabsorbent Protein Particles

3.3.1. Protein functionalization by “dry” acylation

The as-received PPC was mixed with MQw to form a 40 wt.% PPC homogenous mixture. The pH of the mixture was adjusted to pH 11 by adding 1M NaOH, to denature the protein. The alkaline PPC mixture was then placed in a reactor connected to a condensation unit, as shown in Figure 8a. The reactor was closed and placed in a preheated oil bath at 70 °C (Figure 8b, step 2). For the PPC acylation, five commonly used acylation agents were tested (SA, BTCA, EDTAD, CA, and EDTA). The acylation agents were gradually added to the mixture through an opening on top of the reactor while maintaining stirring of the mixture (Figure 8b, step 2). For all reactions, the selected mass ratio (protein:acylation agent) was kept at 0.5:1, based on previous literature on WG “dry” acylation.^[109, 121] The acylation agents were added in excess to the protein content to impede possible excessive cross-linking reactions led by the presence of the reagent. The temperature of the reactor was then increased to 100 °C (at an estimated rate of 1 °C/min), and the total time until the ceiling temperature was reached was ~30 min. This first heating ramp aimed to promote gradual evaporation of the water in the

mixture and initiation of the acylation reaction. At this point, a mixture resembling the viscosity of honey was obtained. Thereafter, the temperature of the reactor was further increased to either 120, 140, or 160 °C (at a heating rate of around 10 °C/min). The temperature and stirring were maintained for 1.5 h (Figure 8b, step 3).

To clean the reacted PPC, the reactor was opened and the mixture was poured into a beaker containing 200 mL of MQw (Figure 8b, step 4). The mixture was vigorously mixed until a suspension was formed and then the pH of the mixture (~pH 2-3) was raised to pH 7 using 1M NaOH. The contents of the beaker were filtered using a filter paper (N3) and the PPC was then rinsed with acetone (Figure 8b, step 5). Some reacted PPC showed an increase in water solubility, which made it impossible to perform the cleaning as previously described. Such samples were instead centrifuged after dispersion in 200 mL MQw at 1200 rpm, with no pH adjustment (pH 2-3). The reacted and cleaned PPC pellet was then re-dispersed in fresh 200 mL MQw, neutralized, and filtered as described above. The paste-like reacted PPC (Figure 8b, step 5), was dried overnight in a conventional oven at 50 °C. A reference PPC sample was also prepared following the same protocol as described above, but without addition of the acylation agents (PPC11). The materials were always kept in a silica-gel desiccator before any test. The nomenclature and reaction conditions are summarized in Table 3.

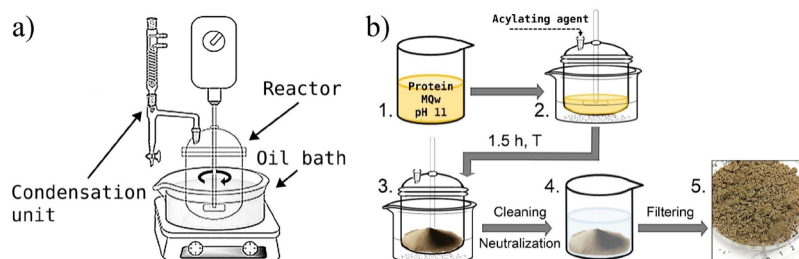


Figure 8. (a) Experimental set-up and (b) preparation procedure for “dry” acylation of potato protein concentrate (PPC). Adapted from Paper IV (2019).^[79]

Table 3. Sample formulations and parameters used in protein functionalization by “dry” acylation.^[79] PPC = potato protein concentrate, SA = succinic anhydride, BTCA = 1,2,3,4-butanetetracarboxylic acid, CA = citric acid (Paper IV).

Sample	Acylating agent	Temperature (°C)
PPC11	None	120
PPC/SA/120	SA	120
PPC/SA/140		140
PPC/SA/160*		160
PPC/BTCA/120	BTCA	120
PPC/BTCA/140*		140
PPC/EDTAD/120	EDTAD	120
PPC/CA/120	CA	120
PPC/CA/140		140
PPC/EDTA/120	EDTA	120

*Samples centrifuged before the neutralization procedure.

3.3.2. Protein functionalization by “wet” acylation

3.3.2.1. Acylation of WG

The as-received WG powder was gradually added to a beaker with MQW (pre-adjusted to pH 11 using 1 M NaOH) until a suspension of 2 wt.% was formed (Figure 9, step 1). The mixture was constantly stirred, the pH was adjusted to pH 11, and gradual WG addition continued for around 10 min. To enable WG denaturation, the suspension was transferred to a water bath, pre-heated to 70 ± 2 °C. The suspension was constantly stirred for 30 min and the temperature of the bath was set to gradually increase to around 90 °C, which was held for at least 5 min. The beaker was then placed in an ice-bath to decrease the temperature to room temperature and the pH of the suspension was adjusted to pH 12 to provide the acylation conditions. For the acylation, 25 wt.% EDTAD (25 g/100 g of EDTAD/WG) was gradually added to the suspension for 30 min (Figure 9, step 2). The pH was monitored using a SevenCompact pH/ion meter (Mettler Toledo, Sweden) and adjusted

to pH 12 when necessary (Figure 9, step 2). The acylation continued for 1.5 h, when no decrease in the pH was evident. For the cleaning, the pH of the treated WG suspension was adjusted to pH 3-3.5 using 1M HCl. The suspension was then centrifuged at 4200 rpm (2000 RCF) for 10 min, and the supernatant was decanted. Freshwater was added to the pellet up to the same volume as before removing the supernatant (Figure 9, step 3). The pellet was broken with a spatula and the suspension was shaken for 10 min. at approx. 2000 rpm (450 RCF), followed by centrifugation. The supernatant was decanted and fresh MQW was again added to the pellet to around 25 % of the initial volume (before centrifugation). The pellet was fragmented with a spatula, vortexed for 10 min, and the pH of the suspension was adjusted to pH 7-8 (Figure 9, step 4). The cleaned acylated WG suspension was poured on glass petri-dishes (Figure 9, step 5), and dried overnight using a forced-air oven set at 50 °C. The films formed were ground to particles using a mortar (Figure 9, step 5). A reference WG sample was also prepared following the procedure described above, but without addition of EDTAD (LC R/WG).

To determine whether the WG acylation efficiency was influenced by the treatment of the protein during industrial drying and concentration (causing possible excessive protein aggregation/cross-linking), an identical sample as previously described was prepared using WGM. The WGM was extracted according to the procedure described in section 3.1. For the analysis, 2 mL of the suspension were removed at each reaction step, i.e., from the alkali treatment to the final cleaned suspension, and the samples were evaluated using size-exclusion liquid chromatography (SE-HPLC), as described in section 3.3.4.

To evaluate the formation of endogenous cross-linking in the WG during acylation, the above protocol was also performed on 8 wt.% WG suspension. To study the importance of the neutralization step, a sample was also produced where the final pH of the suspension was adjusted to pH 11 (instead of pH 7-8). To evaluate the yield after the reaction and cleaning, the protein content of the powders was analyzed using the Dumas method (see

section 3.3.11.). Sample labelling is summarized in Table 4 (except for the control acylation study performed on WGm).

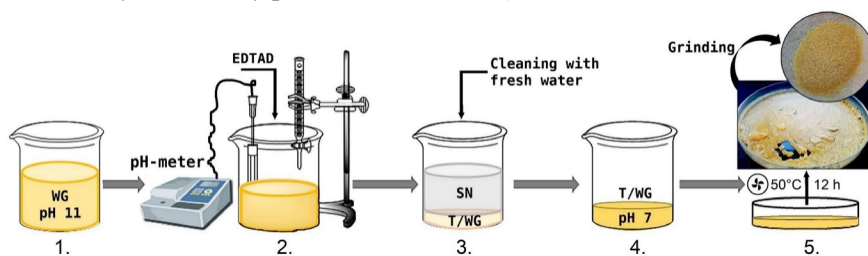


Figure 9. Preparation procedure for “wet” acylation of wheat gluten (WG). Adapted from Paper V.^[86]

Table 4. Sample formulations and parameters used in “wet” acylation of wheat gluten (WG) (Paper V).^[86]

Sample	WG (%)	EDTAD (%)	Final pH	Protein content (%)*
LC R/WG	2	0	7-8	
LC T/WG	2	25	7-8	89.7 ± 0.5
HC R/WG7	8	0	7-8	84.5 ± 0.5
HC R/WG11	8	0	11-11.5	
HC T/WG7	8	25	7-8	88.1 ± 0.1
HC T/WG11	8	25	11-11.5	

*The protein content was measured according to section 3.3.11. The EDTAD (%) is relative to the WG content.

3.3.2.2. Acylation and genipin cross-linking of WG

Acylation of the WG powders followed the same procedure as described in section 3.3.2.1, using 2 wt.% WG in all cases. To evaluate the formation of chemical cross-linking in the acylated WG molecules, after completing the acylation reaction using 25 wt.% EDTAD at pH 12 (relative to the WG content, see section 3.3.2.1.), the temperature of the suspension was increased to 50 °C. Then GEN was added to the suspension to 4 wt.% concentration relative to the WG content. The suspension was stirred at 50 °C for 2.5 h, where a gradual change in color of the suspension was observed, from yellow to light brown (Figure 10a, step 1). The suspension was then cooled to room

temperature, the pH was adjusted to 3.5, and the suspension was centrifuged (Figure 10a, step 2), cleaned, and dried as described in section 3.3.2.1 (Figure 10a, step 3). This sample is referred to as ‘WG25ED4GEN’.

To determine whether addition of GEN before or after acylation played a role in WG network formation, GEN was also added before the acylation reaction on the WG. This sample was prepared as described previously, but the 4 wt.% GEN was added to the 2 wt.% WG aqueous suspension and pre-heated at 50 °C before EDTAD addition. The reaction proceeded for 2.5 h at 50 °C, and a gradual change in color from yellow to dark blue was observed (Figure 10b, step 1). Thereafter, the suspension was cooled to room temperature and the EDTAD acylation, subsequent acidic precipitation (Figure 10b, step 2), cleaning and drying to form a film (Figure 10b, step 3) followed the same process as previously described. This sample is referred to as ‘WG4GEN25ED’. An identically treated WG suspension with 4 wt.% GEN, but without addition of EDTAD, was also produced. It is referred to as ‘WG4GEN’. A summary of sample code, yield, and nitrogen content is given in Table 5.

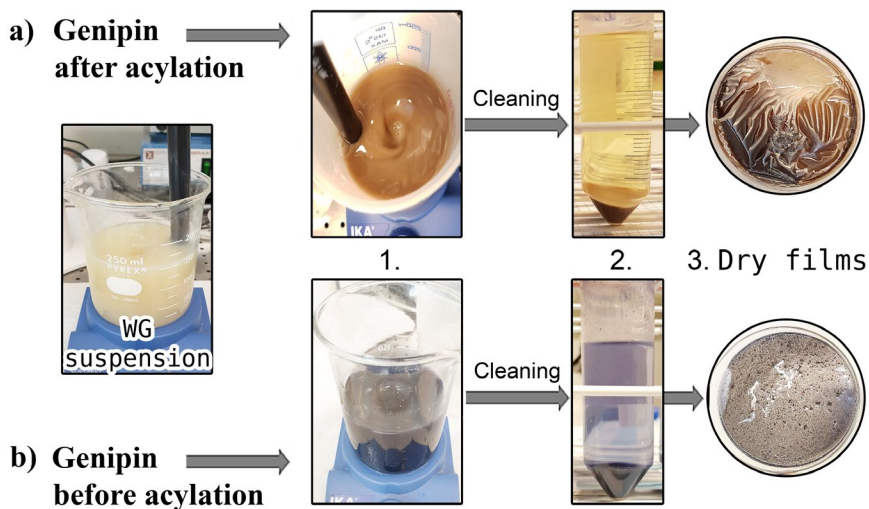


Figure 10. Preparation procedure for acylation and genipin cross-linking of wheat gluten (WG). Adapted from Paper VI.^[116]

Table 5. Sample nomenclature and yield of the different formulations used in acylation and genipin (GEN) cross-linking of wheat gluten (WG) (Paper VI).^[116]

Sample	WG (%)	EDTAD (%)	GEN (%)	Yield (%) [†]	% Protein ^{††}
WG	100				84.8 ± 0.4
WGRef	100			82.5	84.5 ± 0.5
WG25ED	80	20		65.0	89.7 ± 0.5
WG4GEN	96.2		3.85	75.9	
WG25ED4GEN	77.5	19.4	3.10	71.8	81.4 ± 0.6
WG4GEN25ED	77.5	19.4	3.10	70.8	86.4 ± 0.1

*% refer to weight. [†]The dried films were weighed after removal from the oven and the weight was compared to the total initial mass added to each recipe. ^{††}Using the Dumas method and 6.25 as conversion factor.

3.3.2.3. Aqueous acylation of PPC

Acylation of PPC in an aqueous system followed the same process as described in section 3.3.2.1, with some modifications: The EDTAD acylation was prepared with different amounts of EDTAD (5, 10, 15, 20, 25 wt.%) and 1:1, relative to the PPC content. For the cleaning step, the suspensions were directly centrifuged at the reaction pH, without pH adjustment. To evaluate the possibility to functionalize the potato proteins while soluble in the PFJ, i.e., before the extensive PPC aggregation, the process was also performed on as-received PFJ.

To determine whether the PPC acylation efficiency had been influenced by the industrial treatment of the protein, an in-house mild extracted PPC (PPC_m) powder was also used for potato protein acylation as described in section 3.3.2.1. The PPC_m was obtained from fresh potato tubers, as detailed in section 3.1.

3.4. Materials characterization

3.4.1. Free swelling capacity (FSC)

The Non-woven Standard Procedure (NWSP) 240.0.R2, also known as the “tea-bag test”, was used to determine the FSC of the different samples.^[122] Each in-house fabricated bag had dimensions 40 × 60 mm and 25-50 μm pore size (equivalent to 442-305 mesh) and the PET fabric was purchased from Sintab Produkt, Sweden. To prepare the tea-bags, the edges were heat-sealed on three sides and weighed (W_b) before sample insertion. For each test, 100-200 mg of dry sample were inserted (W_d) and the bags were sealed. The filled bags were kept in a desiccator containing silica gel for 12 h before the swelling test. In these tests, the bags were hooked onto a rod and immersed in beakers containing the different test liquids, i.e., MQw, 0.9 wt.% NaCl in MQw (saline solution), Saline A solution (0.9 wt.% NaCl, deionized water, with electrical conductivity 16 mS/cm), defibrinated sheep blood, and 6 M urea in MQw. After the immersion period, the wet bags were hung for 30 s outside the liquid and then placed gently on tissue paper for 10 s to remove excess liquid. The wet bags of sample were measured after 1, 5, 10, and 30 min, and 24 h (W_i). The FSC was determined on triplicates and the results are reported as mean and standard deviation, calculated from Equation 5. To calculate the correction factor (W_{br}), three empty dry bags (W_{db}) were soaked in MQw or saline solution for 24 h and handled as previously described. The wet weight of the empty bags (W_{wb}) was used to obtain the correction factor:

$$W_{br} = \frac{W_{wb}}{W_{db}} \quad (\text{Equation 4})$$

$$FSC \left(\frac{g}{g} \right) = \frac{(W_i - (W_{br} * W_b)) - W_d}{W_d} \quad (\text{Equation 5})$$

To determine the swelling kinetics of the samples, i.e., equilibrium swelling and swelling rate, the Voight equation (Equation 6) was fitted to the swelling data between 1 to 30 min, following the procedure applied by Zhang et al.^[100, 101]:

$$Q = Q_o(1 - e^{-\frac{t}{\tau}}) \quad (\text{Equation 6})$$

where Q represents the absorption at time t (s) in g absorbed liquid/g dry powder, Q_o the maximum absorption after 30 min, and τ the characteristic swelling time in (s).

To determine the liquid spreading properties of the materials, a visual blood absorption test was performed. Around 100 mg of dried powder were evenly distributed on a petri dish and defibrinated blood droplets of $\sim 100 \mu\text{L}$ were gradually added to the material. Each droplet was allowed to soak into the material before adding the next droplet. Liquid addition continued until complete liquid saturation was visually evident (approximately 1 h).

3.4.2. Centrifuge retention capacity (CRC)

The CRC was measured following the standard NWSP 241.0.R. For the test, around 200 mg of powders were placed in an in-house produced tea-bag, in the same manner as for the FSC test described in section 3.3.1., using a swelling time of 30 min. The tea-bags were then centrifuged at 1230 rpm (250 RCF) for 3 min, and the weight of the bags was measured (W_c). The CRC of samples was determined using Equation 7. The CRC of three empty tea-bags was used to obtain the correction factor. Three samples were tested and the mean and standard deviation are reported.

$$CRC \left(\frac{g}{g} \right) = \frac{(W_c - (W_{br} * W_b)) - W_d}{W_d} \quad (\text{Equation 7})$$

3.4.3. Field-emission scanning electron microscopy (FE-SEM)

The particle/foam surface features were examined using an S-4800 field-emission scanning electron microscope (FE-SEM) (Hitachi, Japan). All micrographs were taken using a voltage of 3-5 kV and a current of 10 μA during characterization. The materials were placed on conductive carbon tape and sputter-coated using a 208RH High-Resolution Sputter Coater (Agar, UK) with palladium/platinum (Pt/Pd). Morphological changes in the materials

after swelling were studied by lyophilizing the swollen samples (frozen at -80 °C) for 72 h. A piece of the now foam-like material was then immersed in liquid nitrogen and cryo-fractured. The cryo-fractured pieces were placed on carbon conductive tape and sputter-coated as previously described. The particle size and pore size of the different samples were estimated using the software ImageJ®, taking the average of at least 50 individual measurements.

3.4.4. Size-exclusion high-performance liquid chromatography (SE-HPLC)

Size-exclusion high-performance liquid chromatography analyses were performed using a Waters 2690 separation module and a Waters 996 photodiode array detector (Waters, USA), equipped with a Biosep-SEC-S4000 (300 mm × 4.5 mm) and a prefilter, SecurityGuard GFC 4000 (Phenomenex, USA). To evaluate the extractability/solubility of the materials and the different protein fractions, a three-step extraction procedure was performed following the procedure previously reported by Gällstedt et al.¹⁷⁶ A buffer extraction solution of 0.5 wt.% sodium dodecyl sulphate (SDS) and 0.05 M NaH₂PO₄ (pH 6.9) was used throughout. For the first extraction, 16 ± 0.5 mg of the material were dispersed in 1.4 mL of the SDS-phosphate buffer and shaken at 2000 rpm for 5 min. The dispersion was then centrifuged at 12000 rpm (16000 RCF) for 30 min, and the supernatant was decanted for analysis of the extractable proteins (Ext. 1). For the second extraction (Ext. 2), the remaining pellet from Ext. 1 was resuspended in fresh buffer (1.4 mL), ultra-sonicated (amplitude 5 µm) for 30 s, centrifuged as before, and then the supernatant was decanted for analysis of the extractable proteins. For the third extraction (Ext. 3), the pellet from Ext. 2 was resuspended in 1.3 mL of fresh SDS-phosphate buffer and repeated ultra-sonication steps (30 + 60 + 60 s), with cooling to room temperature between steps, were applied to the suspension. Thereafter, the suspension was centrifuged as before, and the supernatant was decanted and used for analysis of the extractable proteins (Ext. 3). All HPLC analyses were performed in triplicate and the mean and standard deviation are reported.

For the injections, 0.2 mL/min of an isocratic flow consisting of a 1:1 mixture of MQw (0.1 % trifluoroacetic acid, TFA) and acetonitrile (0.1 % TFA) was used as the mobile phase. A 20 μ L aliquot of the respective supernatants from Ext. 1, 2, and 3 were injected. The 3D chromatograms were obtained between 190 and 220 nm, and the chromatogram at 210 nm was used for the analysis. The 210 nm chromatogram was integrated into two fractions as previously reported, i.e., polymeric proteins (PP, from 8 to 18.5 min) and monomeric proteins (MP, from 18.3 to 30 min).

To evaluate the reaction products of EDTAD, GEN, and the combination of these, the reagents were reacted as described in section 3.3.2.2., but without addition of WG. The reaction solutions were lyophilized for 72 h, the resulting foams were ground, and the powders were dissolved in MQw at a concentration of 3 mg/600 μ L. The solutions were diluted to 50% by adding methanol, and the diluted solutions were centrifuged at 7500 rpm (6200 RCF) for 15 min. The solutions were injected into a 1260 Infinity II HPLC, equipped with a Quaternary Pump VL, a UV Diode Array Detector and an LC/MSD detector (Agilent, USA). The column used for the HPLC/LC analysis was an ACE Phenyl (50x3mm, 3 μ L) (VWR, UK). The injections were eluted at 40 °C (1 mL/min), using MQw (0.1 % TFA) and an acetonitrile gradient (from 10 % to 97 %). The prepared samples are referred to as: reacted EDTAD ('rxEDTAD'), reacted GEN ('rxGEN'), and EDTAD/GEN ('rxEDTAD/GEN').

3.4.5. Fourier-transform infrared spectroscopy (FTIR)

Fourier-transformed infrared (FT-IR) spectra were obtained using a Spectrum 100 (PerkinElmer, England), coupled to a Golden Gate single-reflection unit (Graseby Specac LTD, England) and a triglycine sulfate (TGS) detector. The scanning resolution was 4.0 cm^{-1} and data were collected on 32 consecutive scans, from 4000 to 600 cm^{-1} . To follow the protein structural features, the amide I peak (1700-1580 cm^{-1}) was deconvoluted as previously reported by Cho et al.,^[123] using a deconvolution setting of 2 for the enhancement factor (γ) and 70 % for the smoothing filter. The protein

secondary structure fractions were estimated by fitting nine individual Gaussian curves to the deconvoluted amide I curves and using the total area under the curve as a normalization parameter. The peaks for fitting were centered at 1618, 1625, 1634, 1644, 1653, 1667, 1680, and 1691 cm^{-1} , and allowed to move by $\pm 1 \text{ cm}^{-1}$ before completing the final fitting.

3.4.6. Thermal analysis and stability

The thermal stability of the materials was evaluated by thermal gravimetric analysis (TGA) in a TGA/SDTA851 device (Mettler-Toledo, Switzerland), using $14.50 \pm 0.60 \text{ mg}$ of powder placed in alumina crucibles ($70 \mu\text{L}$). The samples were heated to $60 \text{ }^\circ\text{C}$ for 10 min (to reduce the moisture content) and then heated to $800 \text{ }^\circ\text{C}$ ($10 \text{ }^\circ\text{C}/\text{min}$). Nitrogen ($50 \text{ mL}/\text{min}$ flow rate) was always used as the purge gas during the tests.

Differential scanning calorimetry (DSC) was performed on a DSC 820 (Mettler-Toledo, Switzerland) to follow the reaction progression (condensation) of the samples prepared in section 3.3.1. The paste was prepared as described in Figure 8 (step I) and $24.5 \pm 3.5 \text{ mg}$ of the prepared pastes were placed in a punched DSC aluminum crucible ($100 \mu\text{L}$). The DSC method attempted to replicate the conditions in the reactor in section 3.3.1. The method consisted of a heating ramp from 60 to $180 \text{ }^\circ\text{C}$ at a rate of $1 \text{ }^\circ\text{C}/\text{min}$, which simulated the increase in temperature that occurred in the reactor. A nitrogen atmosphere with a flow rate of $50 \text{ mL}/\text{min}$ was maintained for every method.

3.4.7. Compression test

The compression strength of the dry and wet cuboid foam samples from section 3.2.2 was measured using a 5944 Universal Testing Machine (Instron, USA), equipped with a 500 N load cell. To test the wet cuboid samples, the dry foams were swollen in MQw at ambient conditions for 16 h, which is below the maximum swelling time obtained for the foam materials. The dry cuboid specimens were conditioned at 50% relative humidity for 72 h prior

to testing. The dimensions of the foams were measured using a Mitutoyo micrometer. The compression rate used for the tests was 10 mm/min. The mechanical properties were calculated as the average of 3-5 specimens, and the tests were performed at 23 °C and 50% relative humidity, following the ASTM D1621-16 standard. The compression modulus (E , MPa) was calculated as the slope of the linear region, which was typically located below 5% strain. The compressive strength was obtained as the stress at yield when the yield occurred below 10% specimen deformation. If no deflection below 10% of compression was observed (indicating densification of the porous foam), the load was reported as stress at 10%.

3.4.8. Particle charge density

Total charge density of the materials was determined using a 702SM Titrino conductometric titrator unit (Metrohm, Switzerland). To perform the test, the SCAN-CM 65:02 procedure previously described by Hollertz et al.^[124] was used. For this, 0.8 g of sample was dispersed in 50 mL MQw and the pH of the suspension was adjusted to pH 2 to protonate the carboxylic acid groups. The suspension was left under stirring for a maximum of 25 min, to prevent possible protein hydrolysis. To remove excess Na^+ ions from the materials before the conductive titration, the suspension was filtered and then washed several times with MQw until the conductivity of the decanted water was under 0.5 μS . Approximately 0.2 g of the washed material was transferred to a beaker containing 485 mL of MQw, 10 mL 0.1 M NaCl, and 5 mL of 0.01 M HCl. Titration was performed using 0.1 M NaOH in duplicates, with a continuous flow of nitrogen gas.

3.4.9. ^1H nuclear magnetic resonance (^1H NMR)

^1H nuclear magnetic resonance (^1H NMR), 2D correlation spectroscopy (COSY) and Nuclear Overhauser effect spectroscopy (NOESY) were performed at room temperature, using an Advance III HD 400 MHz instrument with a BBFO probe equipped with a Z-gradient coil for structural analysis (Bruker, UK). Data processing was performed in MestreNova

(Mestrelab Research) at a 90° shift square sine-bell apodization window. Baseline and phase correction were applied in both directions.

3.4.10. Time of flight mass spectroscopy (MALI-ToF-MS)

Time of flight mass spectroscopy (MALDI-ToF-MS) was conducted on a UltraFlex MALDITOF-MS equipped with a Scout-MTP Ion Source and an N₂ laser (337 nm) (Bruker Daltonics, Germany). The matrix used was 2,5-dihydroxybenzoic acid (DHB) and sodium was used as a counter-ion.

3.4.11. Protein content analysis

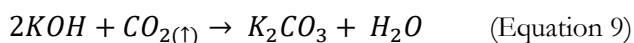
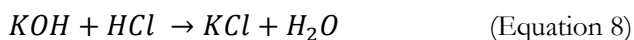
The nitrogen content of the materials was determined following the Dumas method, using a Flash 2000 NC Analyzer (Thermo Scientific, USA). For the test, 3 mg of material were placed in an aluminum capsule, pressed and folded to remove excess air. The capsule was then heated at 1800 °C on an oxidation column, using helium (He) as the carrier. The nitrogen-to-protein conversion factor used was $N \times 6.25$, and the results are reported as the mean and standard deviation for triplicates.

3.4.12. Biodegradation and mold tests

The biodegradability of a commercial SAP, acylated potato protein, and potato starch (as reference) was assessed utilizing soil degradation, following the standard ASTM D5988-03. The soil used for the tests was obtained from a field at SLU, Alnarp (coordinates N55.661303, E13.077222). The soil was sieved to obtain particle size 2 mm and then stored at 5 °C before the test. The moisture content of the soil was estimated by drying ~11 g of the soil at 105 °C for 24 h. The carbon and nitrogen ratio of the materials tested and the soil was obtained as described in section 3.3.11.

For the degradation test, 200 g of soil were placed in an airtight plastic container (1.8 L capacity). To meet the ASTM standard, the pH of the soil was adjusted to pH 6 by adding 10 mL of 0.5M ammonium dihydrogen

phosphate ($\text{NH}_3\text{H}_2\text{PO}_3$), which was also used as a nitrogen source. A beaker containing 50 mL of MQw and a second beaker containing 20 mL 0.5M KOH were also placed inside the plastic container (Figure 11a). Approximately 1 g of powder was homogenously distributed in the soil. A container was also prepared without any sample (blank). The containers were hermetically sealed and stored in a dark room at room temperature. To determine production of CO_2 at a certain time, the containers were opened and the KOH was titrated using 0.25M HCl and phenolphthalein as an indicator. The remaining KOH was stoichiometrically calculated taking into consideration the reaction between HCl and KOH, according to Equation 8. The emitted CO_2 was calculated according to Equation 9. After the titration, a further 20 mL fresh 0.5M KOH were added to the beaker and the container was sealed again for the next measurement.



The mold growing/resistance of SAP, acylated potato protein, potato starch (blank), and wheat gluten powder (reference) was also evaluated. For this, 0.5 g of powder was placed on a petri dish, which was hermetically sealed in a container saturated with MQw (Figure 11b). The moisture uptake of the powders was determined by weighing the samples after 1 week.

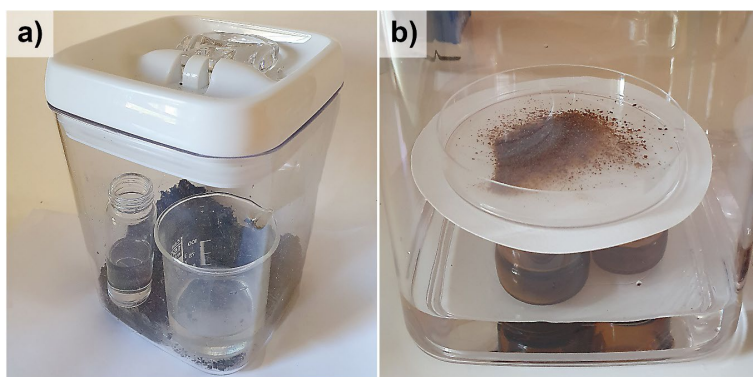


Figure 11. (a) Biodegradation and (b) mold growing experimental set-ups.

4. RESULTS AND DISCUSSION

4.1. Production of WG porous structures

Wheat gluten porous structures were produced using the sedimentation and lyophilization processes. The sedimentation process allowed for production of porous structures with 50-70 % porosity, while the lyophilization process resulted in porous structures with porosity 86-90 %. Liquid uptake by the different porous structures and their structural features were evaluated, with the focus on their ability to perform as a sustainable replacement for the synthetic counterparts used in the personal hygiene industry.

4.1.1. Liquid uptake of the WG-sedimented porous structures

Figure 12 shows liquid absorption by the porous materials produced by the sedimentation process (lyophilization-free). The gradual increase in the water absorption of all recipes, coupled with the increase in foam size with time, indicated the strong effect of water as a plasticizing liquid of the WG, initially absorbed by capillary action and then swelling of the WG cell walls. The highest short (1 s) and long (1 h) water swelling were obtained for the WG/Gly material, whilst the lowest were obtained for WG/high-WG. The maximum water uptake for WG/Gly was ca. 120 % and 480 %, for 1 s and 1 h, respectively (Figure 12a). To evaluate the liquid uptake by solely capillary forces, limonene was used, as this hydrophobic liquid has previously been shown not to contribute to plasticization of WG cell walls.^[93] The fast limonene uptake, above 85 % of the saturation limit within the first 30 s (Figure 12b), and the rapid maximum uptake plateau obtained already after 1 s in many samples, indicated effective inter-connectivity of the pores formed in all materials tested. The well-connected porosity in the foams allowed the material to be fully soaked with limonene within less than 4 s (Figure 12c).

The liquid uptake results showed that the maximum uptake and the uptake rate were a complex function of additives, foam properties (e.g., pore size, porosity), and liquid properties. The high water swelling of WG/Gly and WG/TEMPO was possibly related to the polar nature of the additives contained in these samples (Gly and TEMPO), which contributed to the water swelling capacity of the foams. While WG/high-WG foam had the lowest water uptake, this sample also showed the highest limonene uptake (Figure 12a and b, respectively). This may be a consequence of the denser structure of the WG/high-WG sample compared with the other materials, which may aid in producing higher capillary forces but possibly retard water swelling of the thick cell walls (see section 4.1.2). The water and limonene swelling characteristics of the porous materials resembled those previously reported for WG foams fabricated using lyophilization, suggesting that porous WG-based absorbent materials could be processed using less expensive and less energy-demanding techniques.

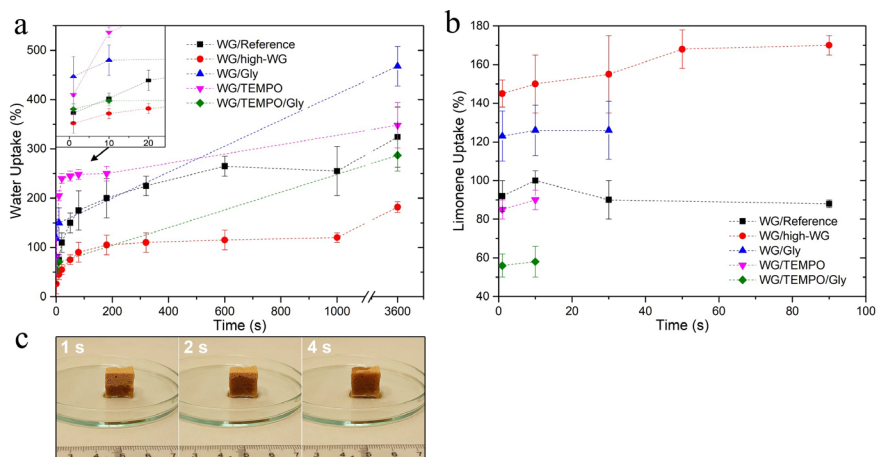


Figure 12. (a) Water uptake and (b) limonene uptake of the different foams, and (c) rapid suction of the WG/TEMPO foam in contact with limonene. Adapted from Paper II.^[112]

Figure 13a shows the sponge effects obtained for the water plasticized WG/TEMPO foam, which could withstand a weight of 2 kg (representing ca. 50 kPa) and recover its shape after removal of the weight. The material could

also be repeatedly compressed without evident physical damage. This property is desirable for applications such as reusable and/or disposable sponges, which are currently mostly fabricated using fossil-based materials. Figure 13b illustrates the same foam saturated in limonene, which did not deform with the load as the limonene was only adsorbed within the porous structure.

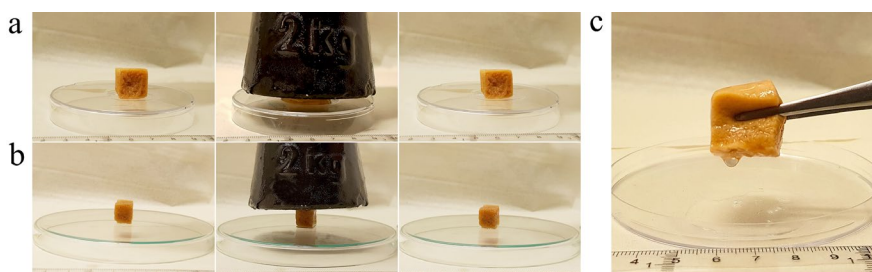


Figure 13. The WG/TEMPO foam exposed to a 2 kg load after saturation in (a) water and (b) limonene. (c) Sponge effect of the material after swelling in water. Adapted from Paper II.^[112]

4.1.2. Liquid uptake of the WG-lyophilized porous structures

The WG foam fabricated using the lyophilization process had an initial water swelling of ~ 6 g/g after 28 min, followed by uptake of ~ 24 g/g after 24 h swelling (Figure 14a). The swollen WG foam increased its volume by around two-fold (compared with the dry foam) and behaved as a cuboid hydrogel (Figure 14c). The swelling agrees with previous swelling results for WG foams.^[93] The use of 1 wt.% CNF resulted in a WG/CNF foam that disintegrated into a slurry-like paste upon contact with water and displayed water swelling below 4 g/g over the entire timespan (Figure 14a and 14d). In contrast, addition of 1wt.% GEN to the WG foam (WG/GEN) resulted in the highest water swelling at 28 min, ~ 18 g/g, and a maximum swelling of ~ 25 g/g at 16 h, corresponding to a 2500% weight increase (Figure 14a and 14e). Although the WG/CNF foam had no cohesion in the wet state, the combination of GEN and CNF resulted in a WG/CNF/GEN foam preserving its shape during water swelling and resulted in a maximum swelling capacity of ~ 10 g/g (Figure 14a and 14f). The difference between the short-

and long-term swelling in WG and WG/GEN was a consequence of the long-term water swelling in the cell walls of the foam due to water plasticization (Figure 14).

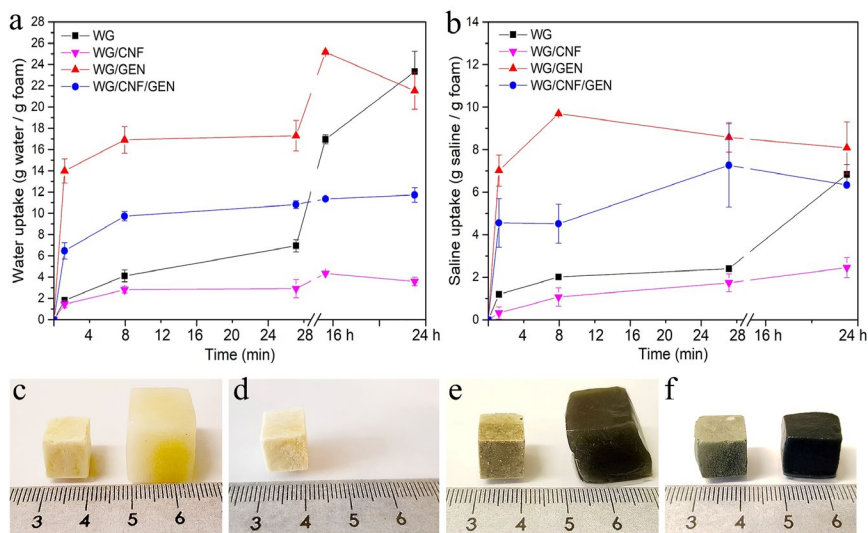


Figure 14. Uptake of (a) water and (b) saline solution by wheat gluten (WG) foams made using genipin (GEN) and cellulose nanofibrils (CNF), and appearance of (left) dry foams and (right) 16 h swollen foams in water of (c) wheat gluten (WG), (d) WG/CNF, (e) WG/GEN, and (f) WG/CNF/GEN. Adapted from Paper III.^[29]

Absorption of saline solution by the WG and WG/GEN foams was lower than the water swelling, resulting in ~ 8 g/g after 24 h swelling (Figure 14b). A decrease in liquid uptake capacity in saline solution has been reported previously for synthetic SAPs, and attributed to a decrease in the osmotic pressure and charge repulsion between the protein network due to the presence of sodium ions in the liquid.^[3] The WG/GEN foam had both rapid water and saline swelling, reaching the maximum capacity at 8 min (Figure 14a and 14b) and with saline uptake ranges similar to some commercial SAPs.

Fitting of the water uptake curve using the Voight equation showed that the WG/GEN foam had the shortest characteristic swelling time ($\tau = 44$ s), in contrast to the WG foam ($\tau = 506$ s). The swelling characteristics of the foams prepared are within the range reported previously for bio-based SAPs

using cottonseed protein grafted with acrylic acid monomers,^[101] despite having no grafted petroleum-based absorbent components. The WG/CNF/GEN foam resulted in a defibrinated sheep blood FSC of ~7 g/g at 10 min, corresponding to 50 % of the total capacity of commercial foams used in sanitary pads. The capillary action in the WG/GEN and WG/CNF/GEN foams was also evaluated as n-heptane uptake at 1 s. Predicted uptake only in the porous structure was estimated (Q_h), using equation 10, and the results are summarized in Table 6. The interconnected channels within the foam structure allowed for rapid uptake of the non-polar liquid, reaching up to 90 % of the maximum predicted uptake during the first second. These results demonstrate the potential of the materials fabricated in this thesis for applications where rapid liquid swelling properties are needed and where commercial products, e.g., sponges and sanitary pads, are today dominated by synthetic materials.

$$Q_h = (V/100 - \nu)(\rho_h/\rho_{WG}) \quad \text{Equation 10}$$

where ν is porosity in (%), ρ_h n-heptane density (684 kg/m³), and ρ_{WG} WG density (1300 kg/m³).

Table 6. Short-term liquid uptake (1s) of the foams fabricated in this thesis. Units are given as g liquid/g dry foam.^{a[29]} Adapted from Paper III.

Sample	Porosity (%)	n-heptane uptake	Water uptake	Q_h (n-heptane)
WG	86 ± 1	2.6	1.8	3.2
WG/CNF	88 ± 0	2.6	2.3	3.8
WG/GEN	86 ± 1	2.4	2.3	4.2
WG/GEN/CNF	90 ± 0	4.2	2.4	4.5

^aDry foam is the weight of the material at 23 °C and 50 % relative humidity.

4.1.3. Structural features of the WG-sedimented porous materials

The WG/Reference material, fabricated solely by phase separation and decanting of the water (sedimentation process), resulted in a porous structure

formed by fused WG agglomerates (Figure 15a). The limonene uptake corresponded to the open structure observed in the SEM micrographs, allowing rapid uptake of the liquid throughout the sample. The WG/high-WG sample resembled the structure of the WG/Reference sample but a denser structure was obtained, with pore size 230 μm compared with 290 μm for WG/Reference (Figure 15b, Table 7). Similar features as for WG/Reference were observed in the WG/Gly, WG/TEMPO, and WG/TEMPO/Gly samples, with the TEMPO-containing materials resulting in a coarser structure, which correlates with the higher density of these compared with WG/Reference (Table 7). The densities observed are within the medium- and high-density foams ranges.^[125]

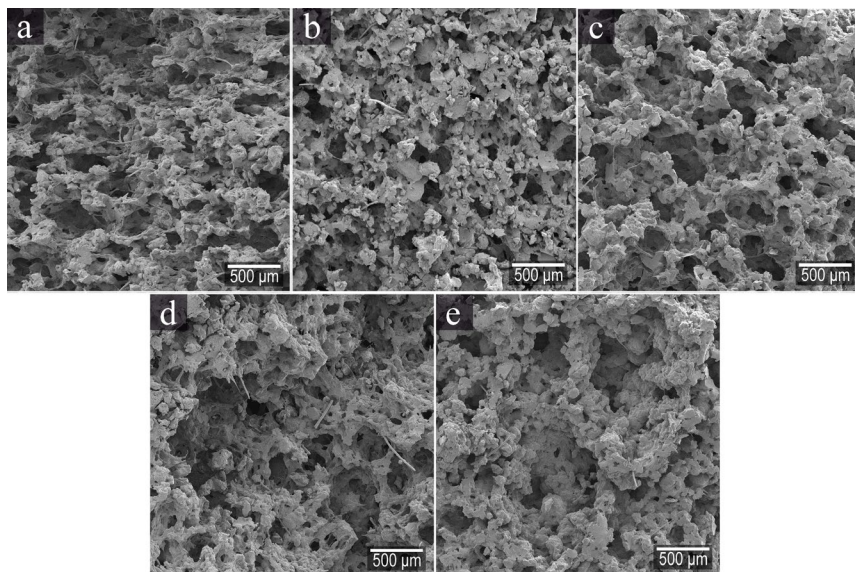


Figure 15. Surface fracture of the sedimented porous structures in (a) WG/Reference, (b) WG/high-WG, (c) WG/Gly, (d) WG/TEMPO, and (e) WG/TEMPO/Gly. Adapted from Paper II.^[112]

Table 7. Physical properties of the foams fabricated by the sedimentation process. Adapted from Paper II.^[112]

Sample	Density (kg/m ³)	Porosity (%)	Pore size (μm)
WG/Reference	370 ± 70	71 ± 5	290 ± 130
WG/high-WG	630 ± 30	52 ± 3	230 ± 60
WG/Gly	370 ± 40	71 ± 3	270 ± 120
WG/TEMPO	590 ± 50	55 ± 4	260 ± 90
WG/TEMPO/Gly	580 ± 30	56 ± 3	270 ± 110

The compression modulus values were highest for the WG/high-WG sample (36 ± 6 MPa), followed by WG/TEMPO, WG/Reference, WG/Gly, and WG/TEMPO/Gly ($E = 12 \pm 3, 5 \pm 1, 0.7 \pm 0.1,$ and 0.4 ± 0.2 MPa, respectively). The high value for the WG/high-WG sample corresponded to the higher density of this sample compared with e.g., WG/Reference (Table 7). The high compressive modulus value for WG/TEMPO demonstrated the reinforcement effect of TEMPO in the WG network, to around three-fold larger compressive modulus than in WG/Reference. The WG plasticization using glycerol corresponded to the low modulus values observed for WG/Gly and WG/TEMPO/Gly, which in turn resulted in foams that could be compressed to the maximum strain tested (80 %) without indication of extensive fracture. The porous structure and the mechanical properties obtained were within the range previously reported for WG lyophilized foams,^[89-93] suggesting that the simple and scalable technique proposed in this thesis allows for production of WG porous structures.

4.1.4. Structural and chemical features of the WG-lyophilized porous structures

The lyophilized WG foam recipes consisted mainly of open cells, with the WG foam having the largest pore size and density among the samples evaluated (Figure 16a, Table 8). The porosity obtained for all lyophilized samples was higher than for foams prepared using the sedimentation process

(Table 7 and Table 8), which partially resulted from complete sublimation of the water crystals during the freeze-drying step, producing smooth structures with well-defined cell walls.^[89, 90, 92] The foams containing GEN, i.e., WG/GEN and WG/CNF/GEN showed holes in the cell walls with connected fibrillar structural features mostly located in the cavities (Figure 16c and 16d, respectively). These samples also had the highest apparent viscosity during mixing of the WG suspension prior to lyophilization of the mixtures (Figure 6). Therefore, the fibrillar structure is considered to be a consequence of the high consistency in the WG/GEN and WG/CNF/GEN mixtures, resulting in areas with extensive elastic stretching during ice formation in the freeze-drying process. The WG/CNF/GEN foam presented a morphology with more holes/fibrillar features, which was reflected in the lowest density (and highest porosity) of this sample compared with WG/GEN (Figure 16d, Table 8).

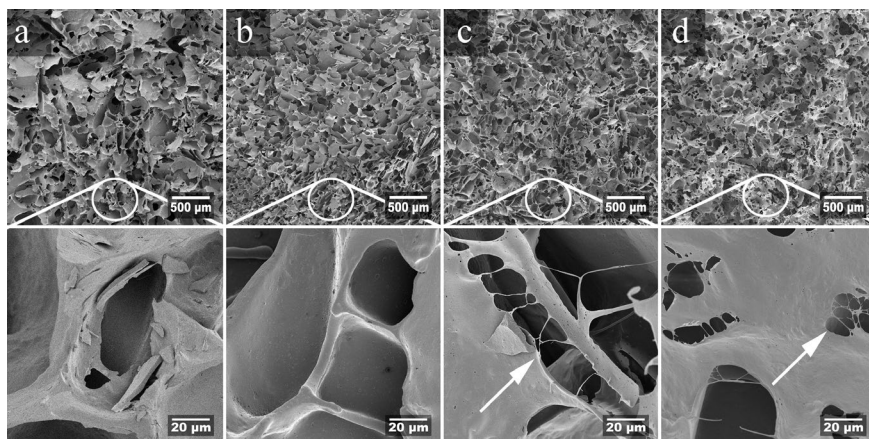


Figure 16. Surface fracture of the lyophilized samples of (a) wheat gluten (WG), (b) WG/CNF, (c) WG/GEN, and (d) WG/CNF/GEN. The arrows indicate fibrillar strands located in the cell walls. Adapted from Paper III.^[29]

Table 8. Physical properties of the foams fabricated using the lyophilization process.^[29] Adapted from Paper III.

Sample	Density (kg/m ³)	Porosity (%)	Pore size (μm)
WG	182±11	86±1	286±67
WG/CNF	159±1	88±0	166±37
WG/GEN	146±10	89±1	167±30
WG/GEN/CNF	135±1	90±0	186±44

The lyophilized WG foam resulted in a compression modulus value of 13 MPa (Table 9), similar to that in the WG foams obtained by the lyophilization-free process (sedimentation). The reinforcement effect of the 1 wt.% CNF in WG/CNF resulted in a foam with around 85 % higher compression modulus (21 MPa) than the WG foam (13 MPa) and at least two-fold higher compression modulus than previously reported for WG reinforced foams with similar densities.^[89, 90, 92] However, the WG/CNF foam showed fragile behaviour during the compression test, where the foam fully fragmented at low compressive strain (<5 %) without any yield (Figure 17a). Addition of GEN alone and/or in combination with WG and CNF did not influence the mechanical properties of the dry foams to a large extent. However, the compression of the WG/CNF/GEN swollen foam resulted in the material not showing apparent yield during the test, whereas the WG/GEN and WG swollen foams broke into gel-like fragments at compressive strains above 50 % (Figure 17b). The WG/CNF/GEN foam could be repeatedly compressed, squeezing out the water, and soaked again in the liquid with a rapid expansion of the material, recovering around 75 % of its original shape during the first 20 s. A similar feature was obtained on soaking the WG/CNF/GEN foam in defibrinated sheep blood, and the behavior resembled the properties of commercial foams used in sanitary pads.

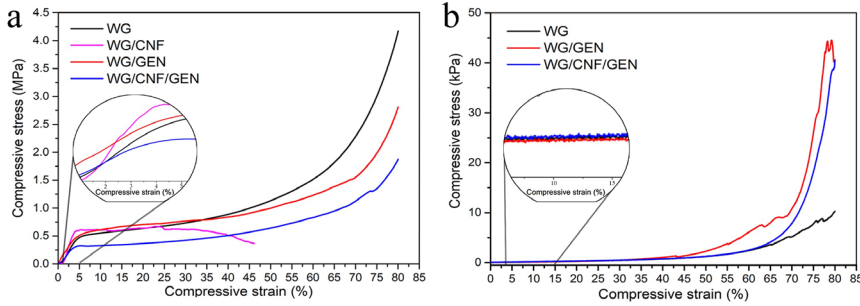


Figure 17. Representative compressive stress-strain curves for (a) the dry foams and (b) the 16 h water swollen foams fabricated from wheat gluten (WG) with genipin (GEN) and cellulose nanofibrils (CNF) using the lyophilization process. Adapted from Paper III.^[29]

Table 9. Mechanical properties of the foams fabricated using the lyophilization process. Adopted from Paper III.^[29]

Dry foam	E (MPa)	σ_s (MPa)	σ_{10} (Mpa)
WG	13.0 ± 1.6	0.42 ± 0.06	0.48 ± 0.05
WG/CNF	20.6 ± 0.8	0.48 ± 0.06	0.48 ± 0.07
WG/GEN	12.3 ± 1.1	0.63 ± 0.24	0.71 ± 0.22
WG/CNF/GEN	13.2 ± 2.4	0.31 ± 0.04	0.32 ± 0.03
Swollen foam	E (kPa)	σ_s (kPa)	
WG	3.7 ± 1.5	0.31 ± 0.09	
WG/GEN	1.3 ± 0.1	0.14 ± 0.04	
WG/CNF/GEN	1.9 ± 0.5	0.22 ± 0.04	

Figure 18a-d show the water swelling in the foam cell walls after 24 h of immersion, which was sublimated during a second lyophilization resulting in a bimodal cell structure. The SEM images of the WG/CNF material after swelling suggest collapse of the foam structure and formation of secondary porosity (below 10 μm size; Figure 18b), corresponding to poor cohesion of the WG/CNF foam after contact with water. The doubly lyophilized WG material preserved most of its original features, besides a developed porous aspect of the cell walls (Figure 18a). The WG/GEN foam showed a random structure with highly porous cell walls (Figure 18c). However, the second lyophilization of the WG/CNF/GEN revealed a structure preserving features of the original WG/CNF/GEN foam (see Figure 16d), but the cell

walls were thicker (above 10 μm) and showed extensive porosity with pore sizes less than 5 μm (Figure 18d). The high resilience of the WG/CNF/GEN foam in the swollen state, coupled with the evident water swelling of the cell walls, suggest an advantage for commercial foams used in sanitary applications. The second lyophilization of a commercial sanitary pad foam (data not shown) did not reveal any secondary porosity formation, indicating that these materials rely only on capillarity uptake and not a combination of both swelling in the cell walls and capillarity.

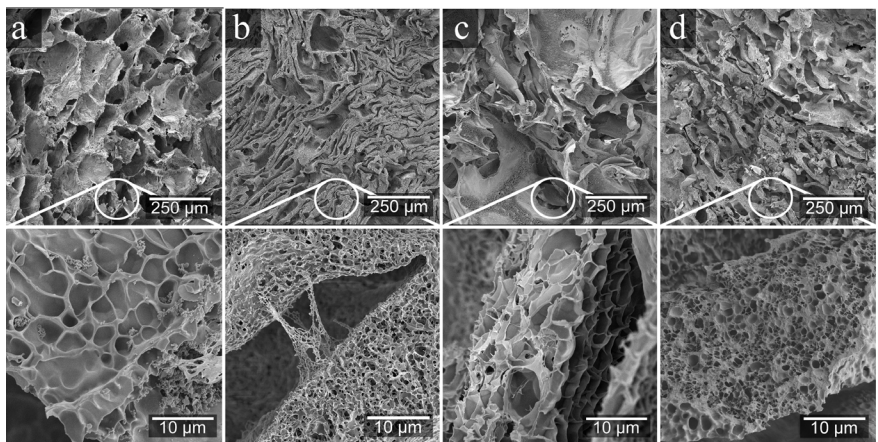


Figure 18. Surface fracture of the lyophilized samples of wheat gluten (WG) with genipin (GEN) and cellulose nanofibrils (CNF), after 24 h water immersion and second lyophilization. (a) WG, (b) WG/CNF, (c) WG/GEN, and (d) WG/CNF/GEN. Adapted from Paper III.^[29]

The evident change in color of the WG/GEN and the material displaying higher swelling properties than the WG foam suggest that GEN not only formed cross-links in the WG, but was also grafted onto the WG, leaving the GEN as a pendant group. GEN is known for primarily reacting to lysine moieties in the protein, forming complexes with oxygen that impart a blue coloring.^[126, 127] However, in cross-linking with protein the GEN molecules form dimers, which could have influenced the cross-linking efficiency as the GEN concentration used (1 wt.%) and the lysine content of WG were low compared with in other GEN-crosslinked proteins.^[128, 129]

The FTIR results for WG/GEN showed that the peak intensity of 1720 and 1440 cm^{-1} of the sample was the highest of all samples (Figure 19a). This suggests that the grafted GEN molecules had also undergone alkali hydrolysis of the methyl ester group contained in the GEN, forming carboxylate/carboxylic acid groups ($-\text{COO}^-/-\text{COOH}$),^[130-132] which in turn contributed to the rapid and high level of swelling observed in this sample (Figure 14a and 14b). The decrease in the high WG/CNF protein extractability during the SE-HPLC extractions when GEN was added to the material in WG/CNF/GEN, from $\sim 60\%$ to 30% (Ext. 1) and 30% to 15% (Ext. 2), indicated that GEN formed a molecular network between the WG and CNF (Figure 19b). The possible reaction between the grafted GEN molecules in the protein and the CNF (also demonstrated here) correlates with the high gel strength and resilient network obtained after the liquid swelling tests, compared with the WG/CNF sample. The suggested reactions in the WG/GEN and WG/CNF/GEN foams are illustrated in Figure 19c and 19d, respectively.

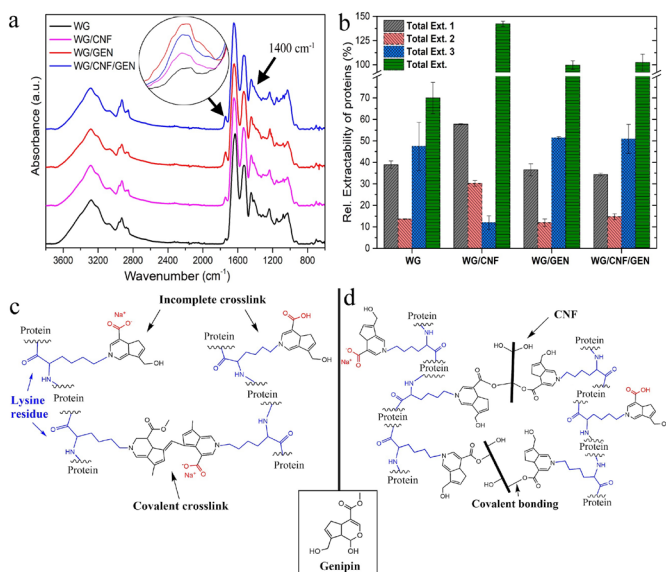


Figure 19. (a) Fourier-transform infrared (FTIR) spectra of material from wheat gluten (WG) with genipin (GEN) and cellulose nanofibrils (CNF). (b) Relative protein extractability and suggested reactions occurring in the (c) WG/GEN and (d) WG/CNF/GEN samples. Adapted from Paper III.^[29]

4.2. Production of solid particle protein-based superabsorbents

The development of SAP materials also involves their production as solid particles, due to certain applications relying on e.g., an SAP powder that is embedded in a cotton pad for baby diapers. Particles from grinding chemically-treated WG and PPC were produced in this thesis. The particles resulted in sizes ranging from 50 to 400 μm , water FSC of up to 36 g/g, and good liquid spreading properties, which are attractive for the development of SAP materials.

4.2.1. PPC superabsorbents based on “dry”-acylation

4.2.1.1. Liquid uptake

The acylated PPC samples, shown in Figure 20a, were characterized by an initial rapid water uptake followed by a gradual FSC increase. The PPC/SA/120 sample reached the highest swelling among the samples tested, with 6 and 13 g/g at 60 s and 24 h, respectively. The same sample, when acylated at 140 °C (PPC/SA/140), resulted in FSC of up to 16 g/g in 24 h (Figure 20b), which indicated that the increase in the acylating temperature aided functionalization of the PPC. The next highest FSC value was seen in the samples treated with BTCA, CA, and EDTAD at 120 °C (Figure 20a), which indicated that each acylation agent, under the conditions applied, provided the protein with different swelling capacities. The SA-treated PPC (PPC/SA/140) also resulted in saline swelling of 4 g/g within 10 min, and CRC double that in the as-received PPC (Figure 20c). The FSC of PPC/SA/120 FSC in water was six-fold larger than for PPC, and three-fold larger than for the reference PPC/11 (Figure 20a and 20d).

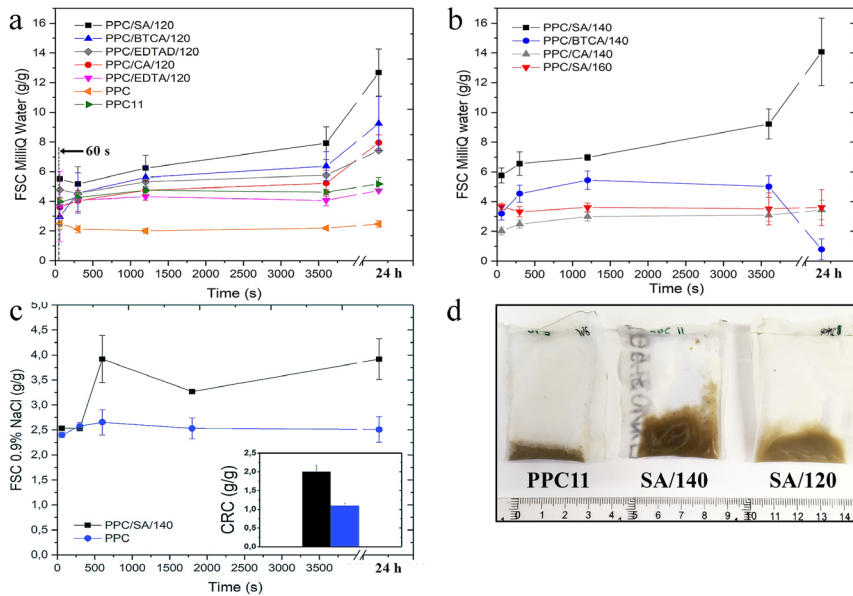


Figure 20. Free swelling capacity (FSC) of the different samples acylated at (a) 120 °C and (b) 140-160 °C in water, and (c) in saline solution. (d) Representative treated potato protein concentrate (PPC) samples during the FSC tests. Adapted from Paper IV.^[79]

Defibrinated sheep blood absorption by PPC/SA/120 was ~5 g/g (30 min), which represents 50 % of the 30 min-blood uptake of commercial synthetic SAPs (10.4 ± 3.1 g/g). Blood uptake by PPC/SA/120 was also 70 % greater than that obtained for PPC, indicating the effects of the SA treatment in increasing the swelling properties of the PPC and improving the potential for using these materials as alternatives to SAPs in e.g., personal hygiene products. The low price of SA, combined with the high PPC concentration, means that this procedure is also attractive for potential industrial scalability.

4.2.1.2. PPC functionalization

The SE-HPLC analysis showed that all acylated PPC samples had higher total protein extractability than the as-received PPC, which is an indication of the increase in protein solubility after acylation (Figure 21a). The SA-acylated sample, which resulted in the highest FSC among the samples produced

(Figure 20a), also had a large Ext. 1 compared with the total relative extractable proteins. Besides, the proteins in PPC/SA/140 were more easily extracted than those in PPC/SA/120 (see Ext. 1 and Ext. 2, Figure 21a), correlating with the lower FSC for the latter sample. In contrast, the acylated PPC samples displayed low FSC values in water (Figure 20), resulting in a high amount of protein extracted during Ext. 2 and 3, i.e., extensive sonication was needed to solubilize the proteins. This suggests that the low FSC of some acylated PPC samples is a consequence of the reagents (e.g., CA, EDTA, EDTAD) cross-linking the protein network, rather than functionalizing the PPC.

Overall, the relative amount of extractable proteins in all acylated samples consisted mainly of polymeric fractions (above 50 %), which was higher than for PPC (Figure 21b). This suggests that cross-linking reactions could also occur in the systems with high FSC, which provides the PPC with a stable network that allows low leakage of the protein during swelling, but also possibly reduces the FSC to some extent. The samples acylated with BTCA and CA at 140 °C, and SA at 160 °C, resulted in a large Ext. 1, which mostly compromised monomeric fractions (above 80 %). These samples leaked extensively from the tea-bag, suggesting extensive hydrolysis of the proteins under the conditions studied.

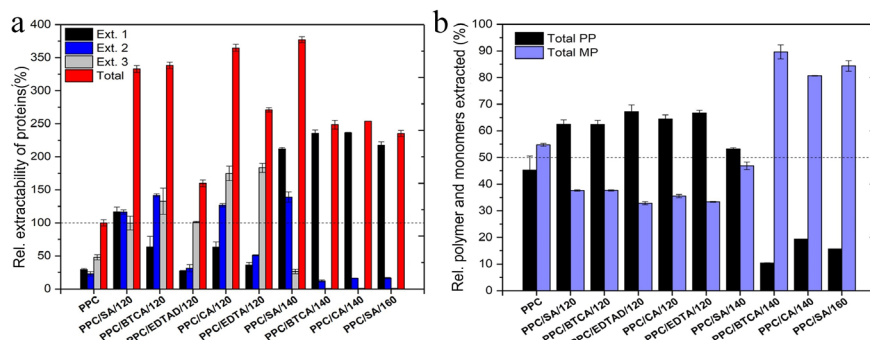


Figure 21. Size-exclusion high-performance liquid chromatography (SE-HPLC) results showing (a) the total relative amount of extractable protein and (b) the relative extracted polymeric (PP) and monomeric (MP) protein fractions. Adapted from Paper IV.^[79]

The FTIR analysis of the BTCA- and SA-acylated PPC showed that the characteristic peaks in the reference treated BTCA and SA (without any protein) were absent, which indicated that cleaning of the samples to remove unreacted salts was effective (Figure 22a). All the acylated PPC showed higher intensity bands at 1730, 1575, and 1390 cm^{-1} , compared with the PPC. The peaks were ascribed to symmetric stretching vibrations of the C=O from carboxylic acid/carboxylate groups (Figure 22a and 22b).^[130, 131, 133] The sharp peak observed for PPC/BTCA/140 at 1730 cm^{-1} indicated an increase in the -COOH groups due to protein hydrolysis, corresponding to the HPLC results (Figure 21).

The conductometric profile of PPC showed the titration of carboxylic acid groups (1st region) and further deprotonation of the amine groups in the protein (2nd region)^[134] (Figure 22c). The PPC/SA/140 sample resulted in a conductometric profile with a single transition region, resembling that of cellulose nanocrystals containing carboxylic acid groups.^[135] This result suggests that the SA in PPC/SA/140 had reacted with most of the lysine groups available in the protein, thereby forming pendant carboxylic acid groups. The estimated increase in the PPC/SA/140 charge density compared with the reference PPC was around 50 % (given in $\mu\text{eq/g}$; Figure 22c). Both materials resulted in similar protein content (using the Dumas method), which demonstrated the effects of SA in increasing the charge density of the protein and thereby contributing to sample FSC.

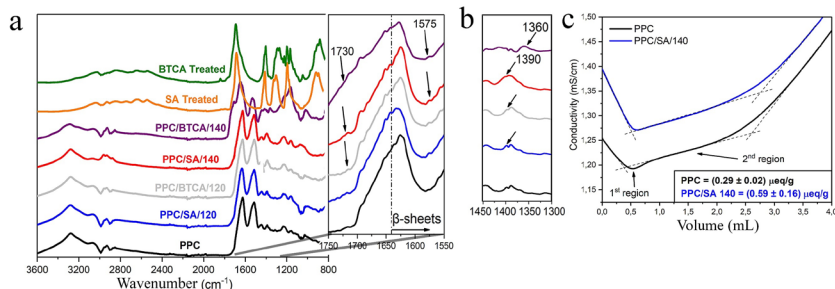


Figure 22. (a) Fourier-transform infrared (FTIR) spectra of the succinic anhydride (SA) and 1,2,3,4-butanetetracarboxylic acid (BTCA) acylated potato protein concentrate (PPC), (b) close-up of the carboxylate region, and (c) conductometric titration representative curves. Adapted from Paper IV.^[79]

The DSC results for identically-prepared mixtures of PPC with the acylation agents (following the sample preparation described in section 3.3.1) showed an endothermic transition in the samples that also gave an increase in the FSC (Figure 23a). This endothermic region was absent in the samples not displaying an important functionalization contribution, i.e., PPC, PPC/EDTA, and PPC/EDTAD. Therefore, the endothermic area was ascribed to both water release/evaporation from the condensation reaction between the protein and the most effective acylation agents (SA, BTCA, and CA), as well as cross-linking reactions possibly occurring in some systems such as PPC/CA (as shown in the HPLC results; Figure 21).

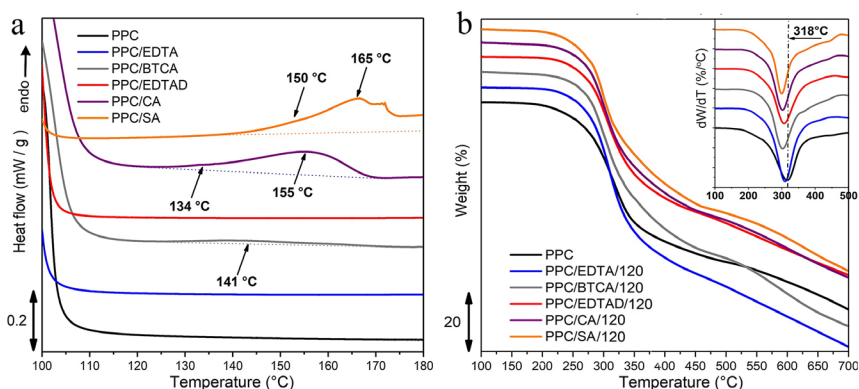


Figure 23. (a) Differential scanning calorimetry (DSC) results for the reaction progress and (b) thermal gravimetric analysis (TGA) results for the acylated potato protein concentrate (PPC). Adapted from Paper IV.^[79]

The DSC analysis also showed that the endothermic range was dependent on the acylation agent used (Figure 23a). For instance, SA showed the highest FSC when acylated at 140 °C, but the acylation at 160 °C produced a sample that leaked from the tea-bags due to extensive hydrolysis (not shown). Both temperatures were within the endothermic region for the PPC/SA system (Figure 23a). This indicates that the observed DSC transition in this sample was a combination of the reaction scenarios occurring, i.e., acylation, cross-linking, and further hydrolysis at higher temperatures. The decrease in thermal stability of the samples compared with PPC (318 °C),

which was the lowest for PPC/SA and PPC/BTCA (300 °C, Figure 23b), demonstrated the structural changes occurring in the protein due to changes in the molecular density after the acylation, as suggested previously.^[136]

4.2.1.3. PPC particulate structure

The samples showed a particle structure with sizes ranging from 10 to 600 μm , and high magnification of the particles did not reveal cavities on their surface (Figure 24). Thus, they resembled the surface of commercial synthetic SAPs. This indicates that the major liquid uptake mechanism corresponded to swelling of the particles, and not capillary forces. The fraction of small size particles observed in Figure 24 could also have influenced the swelling of these samples, as the particles could pass through the mesh of the tea-bags. The phase contrast observed for PPC/BTCA/140 and PPC/SA/140 (Figure 24a and 24c, respectively) is suggested to be a sample topography artefact and/or region with high crystallinity.

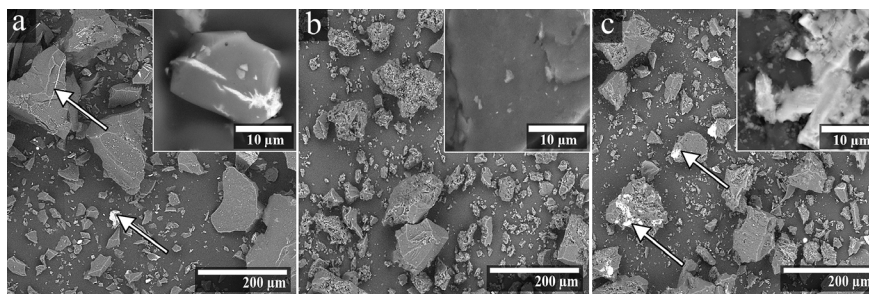


Figure 24. Particle morphology of samples (a) PPC/BTCA/140, (b) PPC/SA/140, and (c) PPC/SA/160. The arrows point to the dendritic structures observed. Adapted from Paper IV.^[79]

4.2.2. Solid particle protein superabsorbents based on “wet”-acylation

4.2.2.1. WG/EDTAD particles

4.2.2.1.1. Liquid uptake

The FSC of the acylated WG particles showed that the sample which was functionalized (25 % EDTAD, WG bases) using a 2 wt.% WG solution (LC T (low concentration-treated)/WG) resulted in a material with initial rapid swelling, but a gradual decrease in swelling until a large amount of material was observed leaking from the tea-bag (Figure 25a). This decrease in swelling was not seen for the reference sample (no EDTAD, LC R/WG), indicating that the lack of a cohesive network was a consequence of the EDTAD treatment of WG. Increasing the WG content suspended during acylation to 8 wt.% (HC T/WG7) resulted in a water FSC of 16 and 22 g/g after 30 min and 24 h swelling, respectively (Figure 25a). This indicates that the EDTAD acylation of the WG increased the water swelling by around seven-fold and three-fold compared with the as-received WG and reference HC R/WG7, respectively. The swollen HC T/WG7 had a consistency resembling a soft gel, similar to swollen synthetic SAP particles (Figure 25d). In the reference sample with a high WG concentration at a final pH of 11 (no EDTAD added, HC R/WG11), the FSC reached stable swelling of up to 12 g/g, whereas in the as-received WG it was only 2 g/g. The increase in WG content from 2 to 8 wt.% resulted in a requirement to promote a more stable network in the WG, thereby allowing the formation of an absorbent material that did not extensively leak from the tea-bag.

The highest saline swelling at 30 min was reached with HC T/WG7, followed by HC T/WG11 (Figure 25b). The maximum saline uptake in the acylated-WG of 5 g/g was around three-fold higher than in the as-received WG, and the saline swelling was less dependent on the final pH of the samples after acylation than the FSC in MQw (Figure 25a). The differences in swelling capacities between the samples neutralized after treatment and those dried at

high pH (HC T/WG7 and HC T/WG11) are possibly a consequence of deamidation of the protein and/or differences in the chemical and structural factors of the protein network, as previously reported for SAP systems.^[8, 85, 137]

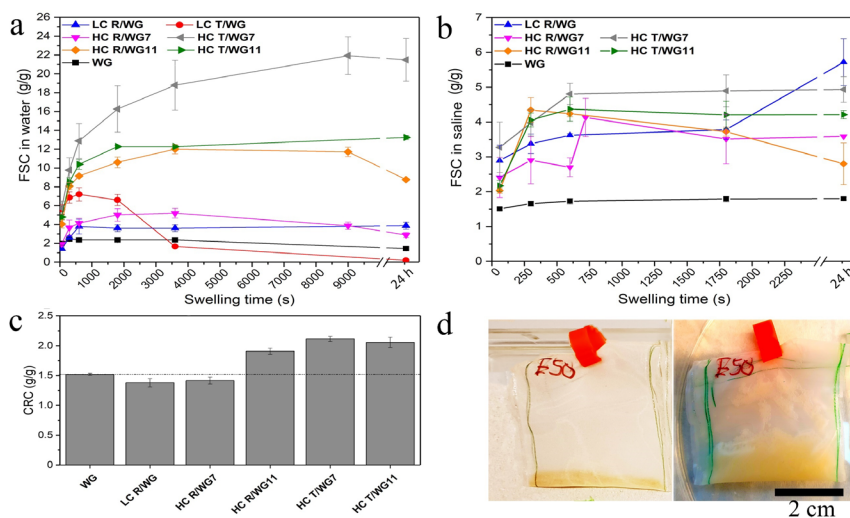


Figure 25. Free swelling capacity (FSC) in (a) MilliQ water (MQw) and (b) saline solution, and (c) centrifuge retention capacity (CRC) after 30 min swelling in saline. (d) HC T/WG7 before and after 24 h MQw swelling. Adapted from Paper V.^[86]

The CRC value was highest for WG T/WG7 and WG T/WG11 (2.1 g/g), followed by HC R/WG11 (1.8 g/g) (Figure 25c). The CRC values for the former samples represented an increase of around 35 % compared with the as-received WG, and indicated that 50 % of the swollen saline liquid was effectively contained within the WG network. The Voight parameters from fitting of the swelling curves revealed that the characteristic swelling time (τ) for the acylated WG materials was dependent on the test liquid and the final pH of the dried samples (Table 10). The acylated WG material showed τ values within the range reported previously for bio-based superabsorbents and resulted in a lower τ than that of synthetic SAP ($\tau = 201 \text{ s}^{-1}$).^[100, 101] However, the equilibrium swelling of the acylated WG materials was lower than that of synthetic SAPs used in diapers (Table 10).

Table 10. Fitted parameters for the different samples using the Voight equation. Adopted from Paper V^[86].^a

Liquid	Sample	Q ₀	τ (s)	R ²
Water	WG	2.36 ± 0.01	33.60	0.998
	LC R/WG	3.63 ± 0.18	175.13	0.962
	HC R/WG7	4.85 ± 0.28	185.52	0.950
	HC R/WG11	11.74 ± 1.00	216.92	0.961
	HC T/WG7	17.45 ± 1.40	306.75	0.935
	HC T/WG11	11.78 ± 0.68	193.05	0.951
Saline	WG	1.73 ± 0.03	29.17	0.995
	LC R/WG	3.59 ± 0,09	36.82	0.989
	HC R/WG7	4.13 ± 0.01	68.63	0.911
	HC R/WG11	4.12 ± 0.19	82.71	0.972
	HC T/WG7	4.57 ± 0.24	48.17	0.958
	HC T/WG11	4.26 ± 0.06	85.40	0.998
	SAP	59.15 ± 1.56	201.61	0.995
Urea	HC R/WG7	10.40 ± 0.95	418.41	0.963
	HC R/WG11	16.69 ± 0.66	282.49	0.990
	HC T/WG7	21.70 ± 2.04	284.90	0.941
	HC T/WG11	20.87 ± 0.24	332.23	0.999

^aData fitted between 0 and 30 min of free swelling capacity.

A visual absorption test using defibrinated sheep blood on HC T/WG7 (with 60 min swelling time) revealed that the material was capable of swelling and retaining 3.2 and 2.4 g/g of the fluid, respectively. During the visual absorption test, the sample HC T/WG7 also showed good liquid spreading properties and the blood was evenly distributed throughout the entire material after dosing the blood droplets, which is an important property for SAP used in personal hygiene products (Figure 26a). The swelling of HC T/WG7 in 6M urea was 32 g/g (equivalent to 29.4 cm³/g), representing an increase of 45 %

in swelling compared with the water swelling of this sample (Figure 26b). This effect is suggested to be a consequence of urea denaturing/unfolding the protein network, thereby facilitating network expansion and thus increasing the swelling uptake (Figure 26c). This indicates that the secondary bonds in the protein should be considered during fabrication of protein-based superabsorbents, as these could restrict the maximum swelling capacity of the material.

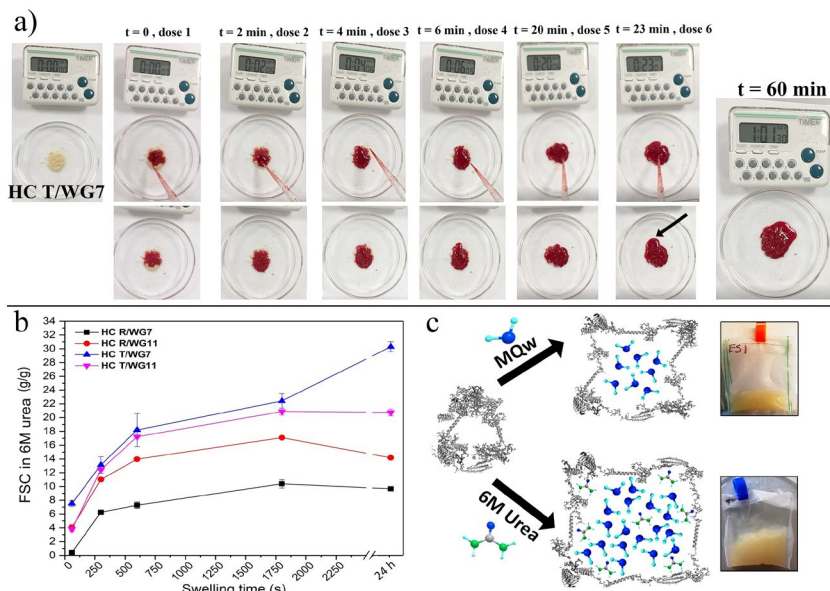


Figure 26. (a) Visual absorption test using defibrinated sheep blood, where the upper row shows a snapshot at dose addition, and the lower row a snapshot around 3 s later (the black arrow indicates liquid saturation point). (b) Free swelling capacity (FSC) of the materials in 6M urea. (c) Conceptual illustration of the effect of urea compared with MilliQ water (MQw). Adapted from Paper V.^[86]

4.2.2.1.2. WG functionalization

The LC T/WG sample had the highest protein extraction among the samples tested, and around 75 % of total extractable proteins was solubilized during Ext. 1 (Figure 27a). This result correlated with the FSC of the sample, which leaked out from the tea-bag due to lack of a stable swollen network, as

also observed for PPC acylation (see Figure 21). The trend corresponded to lower protein extractions for the treated WG samples compared with the as-received WG, suggesting that acid precipitation of the WG during the cleaning step (see Figure 9) possibly contributed to the formation of cross-links and/or additional molecular interactions in the WG. This agrees with previous reports indicating that tyrosine moieties can be ionized, thereby forming dityrosine cross-links in the protein, which reduces their extractability.^[138]

The relative amount of extracted (soluble) polymeric and monomeric fractions in all samples except LC T/WG was similar to that in the as-received WG (Figure 27b). Sample LC T/WG resulted in an extracted polymeric fraction of around 80 %, indicating that the WG it contained was readily solubilized, which correlates with the FSC results. The SE-HPLC results for the supernatant from cleaning the HC T/WG7 material (HC T/WG7 SN) consisted mainly of monomeric protein fractions, which were completely extracted during Ext. 1 (Figure 27), as previously described in section 4.2.1. for the acylated PPC. Furthermore, the Dumas test on the supernatant showed that around 30 % of the solids corresponded to proteins and free-EDTAD (containing nitrogen also). This indicates that most of the weakly bonded proteins were removed during cleaning. The low amount of proteins washed during cleaning is a favorable feature for industrial scalability of the process.

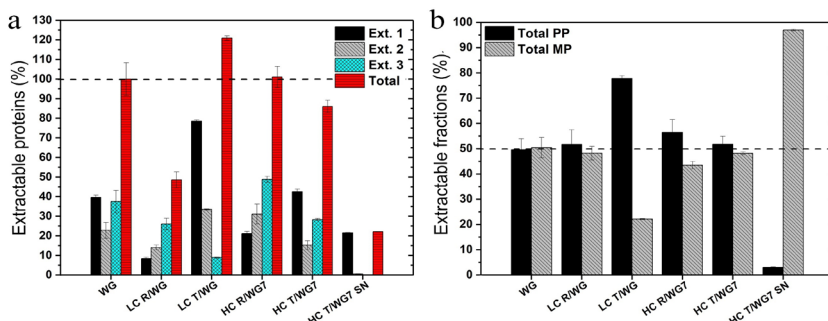


Figure 27. Size-exclusion high-performance liquid chromatography (SE-HPLC) results showing (a) the total relative amount of extractable proteins and (b) the relative extracted polymeric (PP) and monomeric (MP) fractions. Adapted from Paper V.^[86]

All samples showed higher intensity within the carboxylate region, i.e., 1450-1400 cm^{-1} , compared with the as-received WG (Figure 28a). The peak intensity was strongest for HC T/WG7 and HC T/WG11, which suggests that the acylation formed pendant charged carboxylic acid groups on the protein. The condensation of EDTAD on the protein via lysine was further confirmed by the increase in the amide II region intensity (1516 cm^{-1}) for the aforementioned samples, indicating formation of amide bonds following the reaction mechanism illustrated in Figure 4. The conductometric titration after WG acylation showed broadening of the carboxylic acid and amine group deprotonation region, which in turn demonstrated an increase in total charged density groups in the protein after the EDTAD treatment (HC T/WG) (Figure 28b).

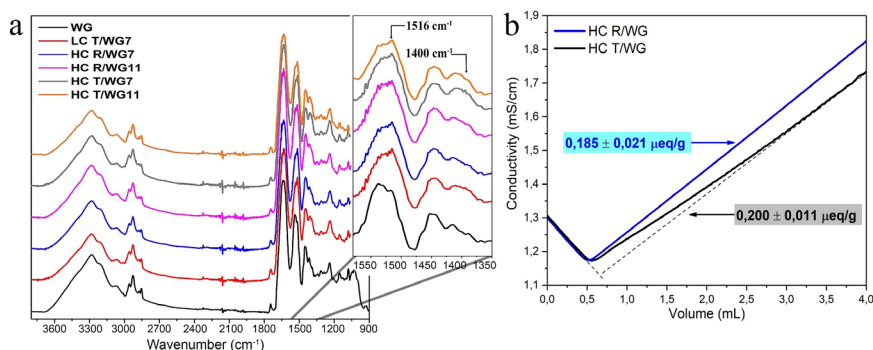


Figure 28. Fourier-transformed infrared (FTIR) spectrograms for (a) the acylated wheat gluten (WG) samples and (b) conductometric titration representative curves. Adapted from Paper V.^[86]

4.2.2.1.3. WG particle structure

The ground acylated WG (HC T/WG7) and the WG reference (HC R/WG7) had particles with sizes $503 \pm 325 \mu\text{m}$ and $290 \pm 153 \mu\text{m}$, respectively (Figure 29). Particulate cross-sections (of the ground dried films) revealed evenly distributed nano-sized pores with diameter ranging from 208 to 395 nm. The nano-sized porosity obtained was associated with the rapid

swelling and liquid spreading properties obtained in the observed samples, suggesting an important capillarity contribution by the pores. The lyophilization of the particles after 24 h saline and 6M urea swelling showed that a foam-like structure had been formed in both cases, and apparent crystalline structures (likely NaCl) were observed embedded in the HC T/WG7 cells walls (Figure 30). This illustrates the high swelling occurring within the WG superabsorbent particulates fabricated in this thesis.

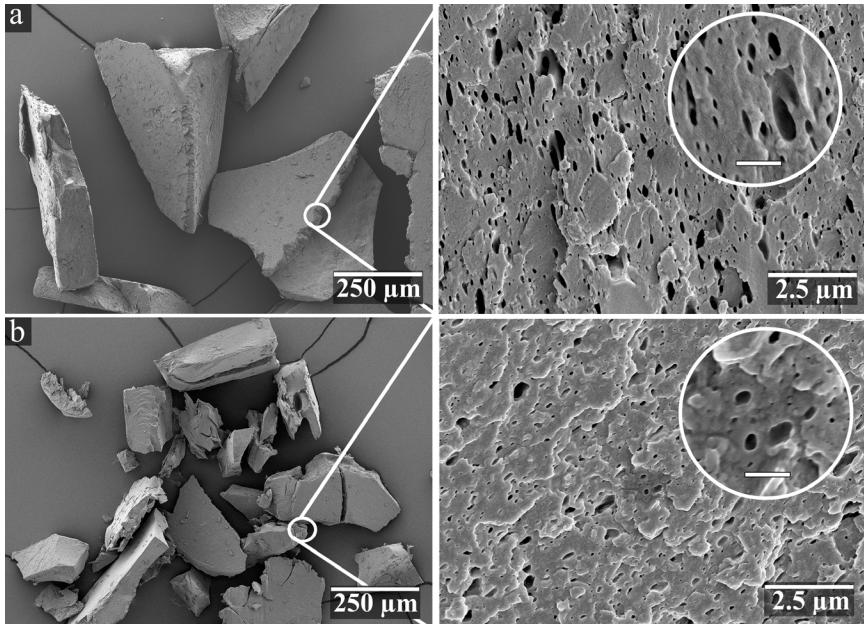


Figure 29. Field-emission scanning electron microscopy (FE-SEM) images of samples (a) HC R/WG7 and (b) HC T/WG7. The high magnification images show the particle cross-sections and the scale bars in the inserts represent 500 nm. Adapted from Paper V.^[86]

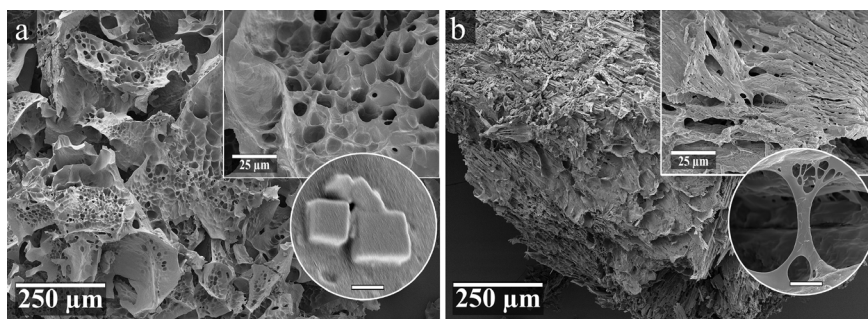


Figure 30. Field-emission scanning electron microscopy (FE-SEM) images of the lyophilized HC T/WG7 particles after 24 h of swelling in (a) saline and (b) 6M urea. The scale bars in the inserts in (a) and (b) represent 400 nm and 2.5 μm , respectively. Adapted from Paper V.^[86]

4.2.2.2. WG/EDTAD/genipin particles

4.2.2.2.1. Liquid uptake

Addition of 4 wt.% GEN after EDTAD acylation of WG (WG25ED4GEN) resulted in a material forming a stable hydrogel after 24 h water swelling, where the material reached an uptake of 36 g/g (Figure 31a). The presence of GEN was demonstrated to produce a network from the acylated WG, which otherwise leaked out from the tea-bag when only EDTAD was used (WG25ED) (Figure 31a and 32c-2). The maximum saline swelling was also highest for WG25ED4GEN, reaching 5.5 g/g after 30 min. The increase in the water and saline 30-min swelling for WG25ED4GEN was 11-fold and up to twofold higher than that of WG and WGRef, respectively. The water uptake was also 64 % higher than for similar WG-based superabsorbents,^[86] demonstrating the important contribution of GEN to both increasing the swelling and forming a network in the treated WG.

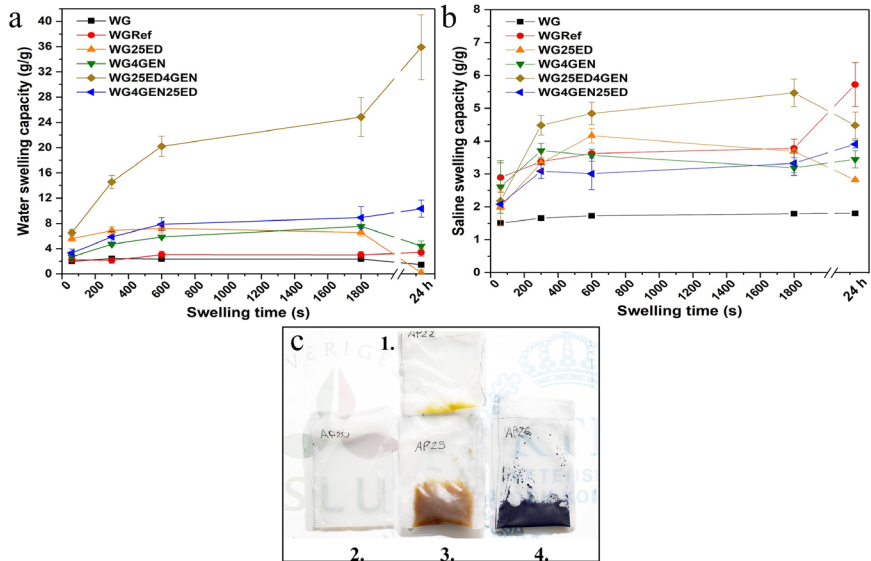


Figure 31. Free swelling capacity (FSC) of the samples in (a) MilliQ water and (b) saline solution. (c) Representative tea-bags containing samples WGRef, WG25ED, WG25ED4GEN, and WG4GEN25ED after 24 h water swelling (1-4, respectively). Adapted from Paper VI.^[116]

The WG25ED4GEN sample resulted in a CRC value of 20.5 g/g in water (Table 11), which indicates that the acylated and GEN cross-linked WG sample was able to retain around 80 % of the water within the protein hydrogel under centrifugation. The sample that was GEN cross-linked before EDTAD acylation (WG4GEN25ED) resulted a CRC value of only 4.9 g/g, due to the GEN cross-linking reaction on the lysine groups reducing the available groups in the protein for the EDTAD reaction. Using only GEN on the WG (WG/4GEN) provided an increase over the WGRef and WG water and saline FSC, suggesting that GEN also provided the protein with charged pendant groups, thereby increasing the liquid uptake. This demonstrates the synergy obtained by the use of the non-toxic GEN in the EDTAD-treated WG, which provided both cross-linking and functionalization of the protein.

Table 11. Centrifuge retention capacity (CRC) of the different samples. Adapted from Paper VI.^[116]

Sample	Liquid	CRC (g/g)
WG	Saline	1.52 ± 0.02
WGRef	Water	1.17 ± 0.10
	Saline	1.37 ± 0.07
WG25ED	Water	Not possible
	Saline	2.72 ± 0.04
WG4GEN	Saline	1.46 ± 0.05
WG25ED4GEN	Water	20.49 ± 0.10
	Saline	2.62 ± 0.20
WG4GEN25ED	Water	4.92 ± 0.20
	Saline	1.53 ± 0.03

4.2.2.2.2. Functionalization mechanisms

The amide II peak at 1525 cm⁻¹ (C=O stretching from amide)^[139] was more intense for all the acylated-WG samples than for WG and WGRef (Figure 32a). Besides, the shoulders observed at 1432-1422 cm⁻¹ and 1395 cm⁻¹ for the WG25ED, WG25ED4GEN, and WG4GEN25ED samples are assigned to carboxylic acid/carboxylate group bands,^[131, 140] indicating the reaction of EDTAD on the lysine residues of the protein, as previously reported. The WG/4GEN sample resulted in an increased intensity at 1078 cm⁻¹ that is ascribed to the stretching of the C-O and/or C-N bonds of the heterocyclic complex formed by the GEN during cross-linking of the WG.^[126, 132] The results obtained agreed with previously reported acylation and GEN cross-linking reaction mechanisms, and the suggested schemes are illustrated in Figure 32b.

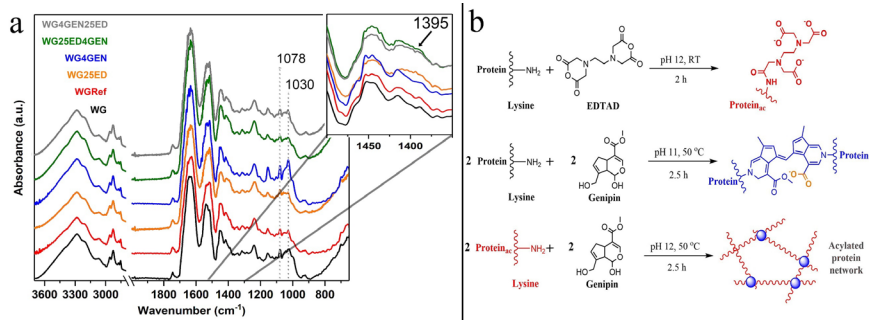


Figure 32. (a) Fourier-transformed infrared (FTIR) spectrograms for the different samples and (b) suggested schemes for protein acylation, wheat gluten (WG) cross-linking with genipin (GEN), and acylated WG cross-linked with GEN. Adapted from Paper VI.^[116]

The reaction with EDTAD under the conditions investigated (rxEDTAD) resulted in a fully ring-opened product (Figure 33a), compared with the ¹H NMR spectra for unreacted EDTAD (Figure 33c). The ¹H NMR results, combined with 2D ¹H COSY NMR, mass spectroscopy, and FTIR results for rxGEN (not shown), revealed that it mainly consisted of a mixture of different complex products from GEN (Figure 33b). Among the products, a double-aldehyde and hydrolyzed GEN product (P1) and an aldol-condensation GEN product (P2) were detected. These polar and charged variations in GEN structures induced by the alkaline and elevated temperature conditions applied to the systems agreed with the superior swelling properties obtained for the GEN-treated materials. A suggested reaction scheme for the different GEN products is illustrated in Figure 33e. These findings confirm the potential for using GEN as a safe bio-based alternative to toxic cross-linkers, simultaneously providing crosslinking and functionalization of the protein, which is beneficial in the design of environmentally friendly superabsorbents.

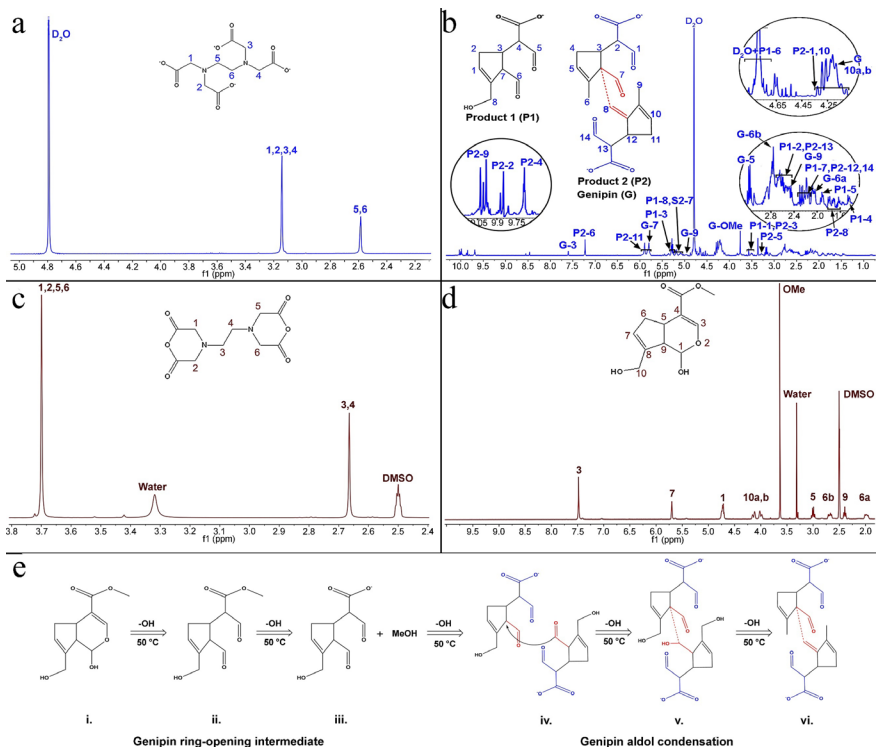


Figure 33. ^1H nuclear magnetic resonance (^1H NMR) results for the samples (a) rxEDTAD, (b) rxGEN, (c) EDTAD, and (d) GEN. (e) Suggested genipin (GEN) aldol condensation reaction. Adapted from Paper VI.^[116]

4.2.2.2.3. Particle structure

The WG25ED4GEN and WG4GEN25ED particulates had estimated dimensions of 340 ± 195 and 267 ± 155 μm , respectively (Figure 34), resembling SAP particle size ranges. Nano-size porosity features with ca. 300 nm diameter were also observed in the samples, as previously shown for the HC T/WG7 material. These surface features are beneficial, as they enable rapid liquid swelling in the materials due to capillary forces.

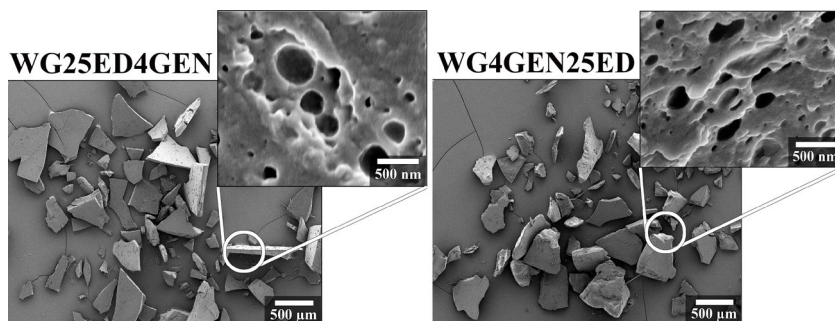


Figure 34. Scanning electron microscopy (FE-SEM) images of the dry particles in samples WG25ED4GEN and WG4GEN25EDTAD. Adapted from Paper VI.^[116]

The lyophilization of the WG25ED4GEN hydrogel after 24 h swelling demonstrated the high uptake occurring in the material, which lost its particle shape and resulted in a foam structure (Figure 35). The interconnected pores were formed due to the sublimation of water crystals contained within the hydrogel, and the cell wall thickness ranged from 500 to 600 nm. Moreover, an apparent fusing of individual hydrogel particles was observed in the SEM image (Figure 35). This agrees with previous reports of “water-welding”/fusion of WG foams when exposed to water.^[90]

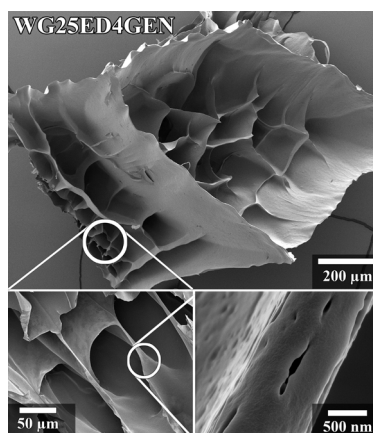


Figure 35. Scanning electron microscopy (FE-SEM) images of the lyophilized WG25ED4GEN sample after 24 water swelling. Adapted from Paper VI.^[116]

4.2.2.3. PPC/EDTAD particles via aqueous acylation

Aqueous acylation of PPC using EDTAD resulted in a material with FSC above 15 g/g within the first 30 min of water swelling. The FSC of the aqueous acylated PPC increased with increasing EDTAD concentration, and was highest for 25 wt.% of EDTAD relative to the PPC content. The maximum saline swelling was around 9 g/g, which represented the highest uptake among the samples fabricated, and was obtained within the first minute. An advantage of using the industrial PPC co-stream is that its low solubility in water facilitated separation and cleaning after EDTAD acylation, and the high degree of endogenous cross-links in the PPC allowed a sufficiently stable network without addition of any chemical cross-linker. A representative hydrogel sample is compared with the as-received PPC in Figure 36.



Figure 36. (left) As-received potato protein concentrate (PPC) and (right) aqueous acylated PPC after 24 h water swelling.

The in-situ acylation of the industrial PFJ and further autoclaving of the juice to promote protein aggregation resulted in an FSC of ~ 10 g/g. Although the FSC was lower than that sample than for the acylated PPC, the results indicate that direct acylation of PFJ is advantageous for designing a functionalization process with a reduced environmental impact.

4.3. Upscaling production of porous WG structures

The swelling characteristics of the different samples prepared using extrusion of WG were dependent on the sample composition and extrusion temperature (Figure 37). Overall, the swelling in water for both low-temperature (LT) and high-temperature (HT) systems showed two swelling scenarios, at 30 min and 24 h (Figure 37a, 37b). The behavior resembled that previously reported for lyophilized foams,^[29] where the first uptake is related to capillary forces and the second to plasticization/absorption effects on the WG. The highest FSC in water was in WG 5S HT (1 g/g and 2.9 g/g after 30 min and 24 h, respectively) (Figure 37b). The large water uptake was illustrated by the increase in the sample volume, as shown for representative extruded samples in Figure 36c and 36d. Likewise, the WG 5S HT sample showed “sponge-like” behavior, and the material could be repeatedly compressed removing the water and re-absorbing it. However, not all the samples showed such behavior, which was generally observed for the samples extruded at high temperature (HT).

Figures 37a and 37b show limonene uptake by the different samples, with the maximum uptake of this non-polar liquid reached already at 10 min. The rapid uptake obtained illustrated the interconnected porosity obtained in the WG materials by the extrusion process and the induced foaming by water evaporation and/or sodium bicarbonate degradation. However, the highest limonene uptake was observed for WG HT (0.3 g/g), which was lower than for previously discussed porous materials obtained using the lyophilization and phase-separation (sedimentation) processes.^[29, 112] The uptake of defibrinated sheep blood was highest for WG 5G5S LT at 0.4 g/g. Examination of the sample cross-section after blood swelling revealed that the red coloring from the blood was mostly located on the outer surface of the extruded sample (Figure 36e). The low liquid penetration to the inner core of the extrudate material explained the reduced liquid uptake of the materials.

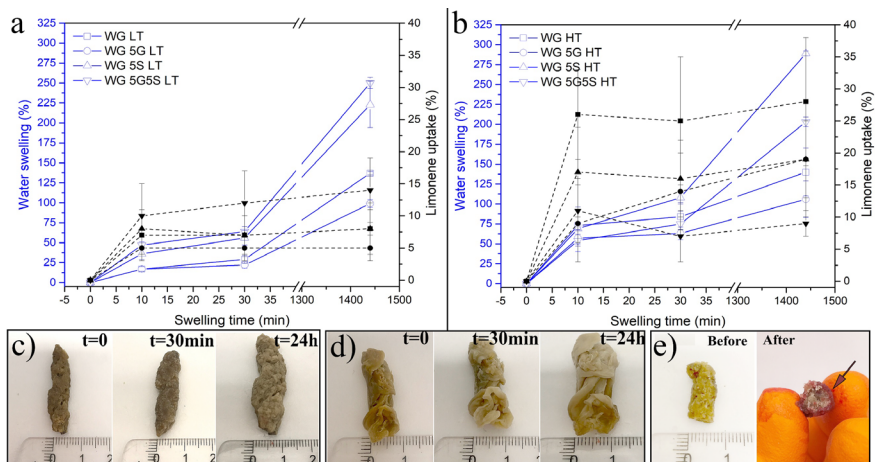


Figure 37. Free swelling capacity (FSC) of the different samples at (a) low (LT) and (b) high (HT) extrusion temperatures in MilliQ water (MQw) and limonene. Representative images of samples (c) WG 5G5S LT and (d) WG 5S HT after 24 h swelling, and (e) cross-section of WG 5G5S LT after 30 min defibrinated sheep blood swelling. Adapted from Paper VII.^[118]

The cross-section images revealed a dense skin located in the outer layer of the WG 5G LT sample, while there was a more porous structure towards the sample core (Figure 38a). Sample WG 5S HT also showed a dense skin feature, but with large and collapsed pores (Figure 38b). The dense skin feature had a thickness of 500 μm and correlated well with the low liquid uptake results obtained for these samples. Figure 38 also shows the microstructure of these two materials after 24 h water swelling and further lyophilization. The swelling of the dense skin and further sublimation of the water crystals resulted in porosity features of ca. 30 μm in size, which in turn illustrated the high-water uptake taking place in the solid extruded WG material.

These samples resulted in the lowest liquid uptake among the samples fabricated within this thesis work. However, the results suggest that the ability to introduce porosity in extruded WG without the utilization of any toxic cross-linker/reagents, while simultaneously using a scalable polymer processing technique, is an attractive solution for fabrication of WG porous

structures displaying liquid swelling capacity. Moreover, it was demonstrated that the swelling capacity of the materials can be tuned by e.g., grinding the extrudate to decrease the effects of the dense skin.

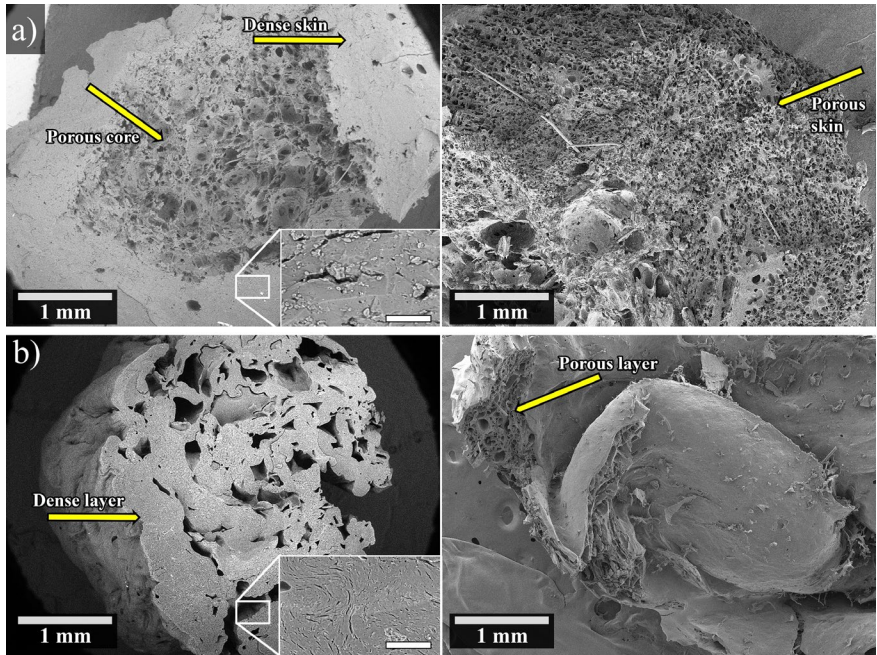


Figure 38. Cross-section of the extruded samples (a) WG 5G LT and (b) WG 5S HT (left) before swelling and (right) lyophilized after 24 h water swelling. Adapted from Paper VII.^[118]

5. Conclusions

Protein-based materials displaying liquid superabsorbency were developed in this work. The materials were fabricated using protein concentrates from industrial agricultural processing co-streams. Two of the largest protein concentrate streams produced in Sweden were studied, i.e., wheat gluten (WG) and potato protein concentrate (PPC). Foams and particle structures were produced, and the performance of the protein-based materials was evaluated for different personal hygiene applications, where both capillary uptake and swelling are required.

WG-based porous structures were obtained by a simple method that consisted of separation of the water phase from WG mixtures. No denaturation, heating, or lyophilization was necessary to produce the WG materials, and the liquid uptake and sample morphology resembled that of freeze-dried WG foams. For fabrication of a stable WG foam, glutaraldehyde was used as the protein cross-linker. The results demonstrated that porous protein-based structures could be produced without using lyophilization, allowing broader possibilities in terms of industrial scalability.

Environment-friendly WG-foams were obtained using the non-toxic protein cross-linker genipin. The genipin-treated WG resulted in foams displaying a stable network and superior liquid swelling compared with the reference WG foams. Synergy in the mechanical and swelling properties was achieved by combining genipin with cellulose nanofibers as a reinforcement agent. The material obtained had properties resembling those of synthetic foams used in disposable sanitary pads.

WG was also functionalized by EDTAD acylation, to increase the material swelling properties and mimic the chemical properties of synthetic superabsorbent polymers (SAPs). The EDTAD acylation resulted in WG particles with similar capacity to absorb water, saline solution, and defibrinated sheep blood as some commercial SAP materials. The

formulations did not involve toxic reagents, and cross-linking of the WG was achieved by endogenous cross-links formed within the WG structure. A unique combination of genipin and EDTAD-acylated WG resulted in particles with superior water swelling (>35 g/g) and liquid retention properties (80 %). These results indicate the potential to improve the liquid swelling properties of protein-based particles by acylating the protein with EDTAD and further cross-linking/functionalizing the material with the non-toxic genipin.

Functionalization tests on PPC using a low-water content recipe revealed that the inexpensive and possibly bio-based succinic anhydride resulted in PPC with improved swelling properties compared with the as-received PPC. Aqueous EDTAD acylation of the PPC was also tested, resulting in a protein-based absorbent material that reached water and saline swelling saturation within the first 30 min. The level of toxins in PPC make it unsuitable for human consumption, and thus for food industry application. Using PPC as a raw material for fabrication of sustainable superabsorbents ensures the availability of raw material for mass production of bio-based SAP in the future.

Extrusion of WG formulations yielded porous structures, demonstrating the possibility to fabricate foamed protein structures using conventional industrial polymer processing techniques. With further optimization, continuous production of sustainable WG porous materials with high liquid swelling capacities is possible. Good potential for producing protein-based materials with SAP properties was demonstrated in this thesis. The work represents an integrated contribution to the UN 2030 sustainable development agenda, and to circular bio-economy principles, as most products currently used in the growing personal hygiene industry (mostly single-use and disposable) are non-biodegradable, use non-renewable resources, and contribute to environmental pollution.

6. Future Work

This thesis demonstrated that the use of industrial protein co-products for fabricating sustainable SAP materials is a promising solution for today's environmentally polluting personal hygiene industry. However, in order to replace synthetic SAPs in the vast range of applications where these materials are used, the following tasks need to be undertaken:

- Osmotic and pressure swelling measurements on the protein-based SAPs to gain a deeper understanding of the swelling mechanisms and the influence of protein structure on liquid uptake.
- Evaluations of the performance of bio-based SAP materials using additional standard industrial tests, e.g., AUL and skin contact.
- Combined protein acylation and foaming coupled with evaluation of the swelling kinetics of the resulting materials.
- An economic assessment of converting from a fully-petroleum based SAP to a fully-protein based SAP disposable item, to determine the industrial feasibility of the materials.
- Work to improve saline uptake and CRC values to the same level as in synthetic SAP used in baby diapers, which is one of today's most demanding application requiring SAP properties.
- Optimization of the extrusion process, e.g., using a controlled water carrier, thereby promoting more homogenous foaming of the samples.
- Evaluation of the protocols at pilot-scale for producing larger amounts of the protein-based materials. This will allow further industrial testing of the materials in different application areas where high liquid absorption/retention capacities and biodegradability are needed.

7. Acknowledgments

Firstly, I would like to acknowledge my family, because they have always been the support that I needed. *A mi madre, quien me ha apoyado y escuchado sin importar mis defectos. A mi papá, que siempre ha querido lo mejor para mí. A mi Segundo padre, que con sus mal chistes me ha alegrado los días. A mi segunda madre, por cuidar a mi papá siempre. A mi nonna Tina, que hasta sus últimos días me levantó con un rico café con leche caliente y que nunca ocultó su desvivido amor por mí. A mis abuelos por siempre tenerme presente.* To my forever partner Wolfgang, who often bore the brunt during my PhD crises, and just always returned love to me. To my unconditional brother from another mother Pierre Larroche, the first person I met when I came to Sweden, and to my little sister Xinchun Ye, who is always there when I need her.

I am deeply grateful to my supervisors: Eva Johansson, Mikael Hedenqvist, Richard Olsson, and William Newson. They have done exceptional work in teaching me the arts of science. They were also very patient when I came to meetings with a thousand unorganized ideas. I would like to thank my funding agency VINNOVA and the companies who were involved in the project: Lantmännen and Essity. Special thanks are given to Annelie Moldin and Malin Lundman, as they dedicated time from their busy agendas to collaborate with me as industrial supervisors. To Bo Rydins Stiftelse for trusting on me and allowing me to continue in Academia.

I have met amazing professors/researchers/collaborators during my scientific career to date, whose have provided me with amazing experiences. I would like to acknowledge Prof. Keiji Numata and his amazing team, for allowing me the opportunity to expend two amazing months in his lab in RIKEN. There, I met exceptional scientists and, above all, amazing friends: Sissi, Neval, Joan, Simon, Shamita, Xiao, Alex, Nam, Fujita, Tsuchiya, Ayumi.

During my work, I had the pleasure to teach and work together with many students, Jean-Christian, Hajar, David, Loris. I had the experience of supervising within my project two highly talented students: David Glad and

Eva Robert, and I thank them for helping out during my work. I would also like to thank my collaborators, whose work helped me to improve my manuscripts: Thomas, Faraz, Oisik, Yuxiao, Eliane. I especially acknowledge my collaborator and friend Qiong Wu, with whom I shared my office and life since I was a Master's student.

I had the pleasure of dividing my PhD studies between two research groups, which meant that I received more than double the love, knowledge, and wisdom! I want to acknowledge all the members from the Product Quality group (SLU) and Polymeric Materials group (KTH). Special thanks to all the staff at the Departments of Plant Breeding and Fibre and Polymer Technology. I take with me more than one pleasant memory from all of you. Thank you, Sophie, Catja, Beata, Alex, Awais, Sbatie, Evelyn, Karina, Jonathan, Vera, Rita, Maja, Salvatore, Xinfeng, Ana (my adoptive Spanish mother and Swedish model), Payam, Hüsam, Maren, Mercedes, Nazanin, Eva, Billy, Óscar, Tomáš, Ann-Sofie, Ramune, Camilla, Marisa, Malin, Märten & Gunborg.

Thank you to “The Bridge” members, for making my office days so much pleasant: Anna-Lovisa, Joel, Lan, Emilia, and Joakim. Thank you to my forever crazy Celia and bestie Chiara. I am truly sorry if I have forgotten to mention someone, but my supervisors have already complained that this thesis is too long!

I would like to acknowledge my home university, Universidad Simón Bolívar, and all its staff, because they taught me all the fundamental knowledge that I needed to start my PhD studies. To my high school “U.E. Colegio El Carmelo” and the teachers/staff who started my early academic development. Thank you to all those friends who I still keep from both institutions, Vanessa F., Natalia, Mariana, Luis, Mauricio, Alonso, Abel, Rodulfo, Gerardo, Samantha, Javier, Vanessa, Betsa, Jainny, Dawniellys, Armstrong, Mike, Sahid, José Daniel, Jesús, Manuel, Mariano, Ylyerid, Marcello, Nicolás, Alí, Laura...

8. References

1. F. L. Buchholz, Preparation Methods of Superabsorbent Polyacrylates. In *Superabsorbent Polymers*, American Chemical Society: Michigan, **1994**; Vol. 573, pp 27-38.
2. F. L. Buchholz; A. T. Graham *Modern Superabsorbent Polymer Technology*. John Wiley & Sons, USA, **1998**, Vol. 1.
3. A. J. Capezza; W. R. Newson; R. T. Olsson; M. S. Hedenqvist; E. Johansson, *ACS Sustain. Chem. Eng.* **2019**, *7*, 5, 4532-4547, DOI: 10.1021/acssuschemeng.8b05400.
4. K. A. Brandt; S. A. Goldman; T. A. Inglin *U.S. Patent 4,654,039*, **1987**.
5. C. Chang; L. Zhang, *Carbohydr. Polym.* **2011**, *84*, 1, 40-53, DOI: 10.1016/j.carbpol.2010.12.023.
6. B. Zavan; R. Cortivo; G. Abatangelo, Hydrogels and Tissue Engineering. In *Hydrogels: Biological Properties and Applications*, Barbucci, R., Ed. Springer Milan: Milan, **2009**; pp 1-8.
7. Y. Zhao; J. Kang; T. Tan, *Polym.* **2006**, *47*, 22, 7702-7710, DOI: 10.1016/j.polymer.2006.08.056.
8. Y. Zhao; H. Su; L. Fang; T. Tan, *Polym.* **2005**, *46*, 14, 5368-5376, DOI: 10.1016/j.polymer.2005.04.015.
9. M. J. Zohuriaan-Mehr; K. Kabiri, *Iranian Polym. J.* **2008**, *17*, 6, 451-477.
10. C. M. Garner; M. Nething; P. Nguyen, *J. Chem. Educ.* **1997**, *74*, 1, 95, DOI: 10.1021/ed074p95.
11. A. B. Kinney; A. B. Scranton, Formation and Structure of Cross-Linked Polyacrylates. In *Superabsorbent Polymers*, American Chemical Society: **1994**; Vol. 573, pp 2-26.
12. A. Adair; A. Kaesaman; P. Klinpituksa, *Polym. Test.* **2017**, *64*, 321-329, DOI: 10.1016/j.polymertesting.2017.10.018.
13. A. V. Dobrynin; M. Rubinstein, *Progr. Polym. Sci.* **2005**, *30*, 11, 1049-1118, DOI: 10.1016/j.progpolymsci.2005.07.006.
14. U. W. Gedde, Polymer Solutions. In *Polymer Physics*, Springer Netherlands: **1999**; Vol. 1, pp 55-75.
15. J. P. Haar Jr.; R. J. Ross *U.S. Patent 5,998,492*, **1999**.
16. A. T. Horvath; A. E. Horvath; T. Lindström; L. Wägberg, *Langmuir.* **2008**, *24*, 19, 10797-10806, DOI: 10.1021/la800669d.
17. M. Sadeghi; H. Hosseinzadeh, *Bras. J. Chem. Eng.* **2013**, *30*, 379-389.
18. F. Horkay; I. Tasaki; P. J. Bassar, *Biomacromolecules.* **2000**, *1*, 1, 84-90, DOI: 10.1021/bm9905031.
19. J. Rodenburg; M. Dijkstra; R. van Roij, *Soft Matter.* **2017**, *13*, 47, 8957-8963, DOI: 10.1039/C7SM01432E.
20. J. Barrat; F. Joanny, Theory of Polyelectrolyte Solutions. In *Advances in Chemical Physics*, 1 ed.; Rice, P. a. S. A., Ed. Wiley **2007**.

21. A. Isogai, Pretreatment of Cellulose for Further Processing. In *Handbook of Green Materials*, World Scientific: **2013**; Vol. Volume 5, pp 35-51.
22. A. Isogai; T. Saito; H. Fukuzumi, *Nanoscale*. **2011**, *3*, 1, 71-85, DOI: 10.1039/C0NR00583E.
23. M. Nagasawa, Introductory Remarks. In *Physical Chemistry of Polyelectrolyte Solutions*, Nagasawa, M., Ed. John Wiley & Sons: New Jersey, **2015**; Vol. 158.
24. M. Nagasawa, Thermodynamic Properties of Polyelectrolyte Solutions. In *Physical Chemistry of Polyelectrolyte Solutions*, Nagasawa, M., Ed. John Wiley & Sons: New Jersey, **2015**; Vol. 158.
25. P. J. Flory; J. Rehner, *J. Chem. Phys.* **1943**, *11*, 11, 521-526, DOI: 10.1063/1.1723792.
26. P. J. Flory; J. Rehner, *J. Chem. Phys.* **1943**, *11*, 11, 512-520, DOI: 10.1063/1.1723791.
27. T. Tanaka; D. J. Fillmore, *J. Chem. Phys.* **1979**, *70*, 3, 1214-1218, DOI: 10.1063/1.437602.
28. H. Omidian; S. A. Hashemi; P. G. Sammes; I. Meldrum, *Polym.* **1998**, *39*, 26, 6697-6704, DOI: 10.1016/S0032-3861(98)00095-0.
29. A. J. Capezza; Q. Wu; W. R. Newson; R. T. Olsson; E. Espuche; E. Johansson; M. S. Hedenqvist, *ACS Omega* **2019**, *4*, 19, 18257-18267, DOI: 10.1021/acsomega.9b02271.
30. F. A. L. Dullien, Structure of Porous Media. In *Transport Processes in Porous Media*, Bear, J.; Corapcioglu, M. Y., Eds. Springer Netherlands: Dordrecht, **1991**; pp 3-41.
31. K. Kabiri; H. Omidian; M. J. Zohuriaan-Mehr, *Polym. Int.* **2003**, *52*, 7, 1158-1164, DOI: 10.1002/pi.1218.
32. K. Kabiri; H. Omidian; M. J. Zohuriaan-Mehr; S. Doroudiani, *Polym. Composite*. **2011**, *32*, 2, 277-289, DOI: 10.1002/pc.21046.
33. Q. Xiong; T. G. Baychev; A. P. Jivkov, *J. Contam. Hydrol.* **2016**, *192*, 101-117, DOI: 10.1016/j.jconhyd.2016.07.002.
34. F. A. L. Dullien, 4 - Selected Operations Involving Transport of a Single Fluid Phase through a Porous Medium. In *Porous Media (Second Edition)*, Academic Press: San Diego, **1992**; pp 319-332.
35. F. A. L. Dullien, 2 - Capillarity in Porous Media. In *Porous Media (Second Edition)*, Academic Press: San Diego, **1992**; pp 117-236.
36. L. Brannon-Peppas; N. A. Peppas, The Equilibrium Swelling Behavior of Porous and Non-Porous Hydrogels. In *Absorbent Polymer Technology*, Brannon-Peppas, L.; Harland, R. S., Eds. Elsevier: Amsterdam, **1990**; Vol. 8, pp 67-102.
37. P. Bajpai, Miscellaneous Topics. In *Biermann's Handbook of Pulp and Paper (Third Edition)*, Bajpai, P., Ed. Elsevier: **2018**; pp 493-516.
38. J. R. Ajmeri; C. J. Ajmeri, Developments in the use of nonwovens for disposable hygiene products. In *Advances in Technical Nonwovens*, Kellie, G., Ed. Woodhead Publishing: **2016**; pp 473-496.
39. S. Damodaran *U.S. Patent 6,310,105*, **2001**.
40. S. Damodaran *U.S. Patent 6,821,331*, **2004**.

41. T. Calafut, Applications of Polypropylene Films. In *Plastic Films in Food Packaging*, Ebnesajjad, S., Ed. William Andrew Publishing: Oxford, **1998**; pp 93-119.
42. M. Cordella; I. Bauer; A. Lehmann; M. Schulz; O. Wolf, *J. Clean. Prod.* **2015**, *95*, 322-331, DOI: 10.1016/j.jclepro.2015.02.040.
43. M. Broeren; I. Odegard LCA of waste treatment of diaper material. <https://www.cedelft.eu/en/publications/2068/lca-of-waste-treatment-of-diaper-material>.
44. N. Castrillon; M. Echeverria Molina; H. Fu; A. Roy; J. Toombs, **2019**, DOI: 10.13140/RG.2.2.15095.98720.
45. E. Johansson; A. H. Malik; A. Hussain; F. Rasheed; W. R. Newson; T. Plivelic; M. S. Hedenqvist; M. Gällstedt; R. Kuktaite, *Cereal Chem.* **2013**, *90*, 4, 367-376, DOI: 10.1094/CCHEM-08-12-0105-FI.
46. E. A. MacGregor; C. T. Greenwood *Polymers in nature*. John Wiley & Sons, Chichester, **1980**.
47. K. P. Murphy, Stabilization of Protein Structure. In *Protein Structure, Stability, and Folding*, Murphy, K. P., Ed. Humana Press: Totowa, NJ, **2001**; pp 1-16.
48. O. Ololade, Classification of Natural Polymers. In *Natural Polymers: Industrial techniques and application*, Ololade, O., Ed. Springer: Switzerland, **2016**; pp 1-17.
49. G. Paradis; F. V. Chevance; W. Liou; T. Renault; K. T. Hughes; S. Rainville; M. Erhardt, *Sci. Rep-UK* **2017**, *7*, 1, 1282, DOI: 10.1038/s41598-017-01302-5.
50. L. Römer; T. Scheibel, *Prion*. **2008**, *2*, 4, 154-161.
51. X. Ye; M. S. Hedenqvist; M. Langton; C. Lendel, *RSC Adv.* **2018**, *8*, 13, 6915-6924, DOI: 10.1039/C7RA10981D.
52. X. Ye; K. Junel; M. Gällstedt; M. Langton; X.-F. Wei; C. Lendel; M. S. Hedenqvist, *ACS Sustain. Chem. Eng.* **2018**, *6*, 4, 5462-5469, DOI: 10.1021/acssuschemeng.8b00330.
53. F. Muneer; M. Andersson; K. Koch; M. S. Hedenqvist; M. Gällstedt; T. S. Plivelic; C. Menzel; L. Rhazi; R. Kuktaite, *ACS Sustain. Chem. Eng.* **2016**, *4*, 12, 6332-6343, DOI: 10.1021/acssuschemeng.6b00892.
54. F. Muneer; E. Johansson; M. S. Hedenqvist; M. Gällstedt; W. R. Newson, *BioResources*. **2014**, *9*, 3.
55. F. Muneer; E. Johansson; M. S. Hedenqvist; T. S. Plivelic; R. Kuktaite, *Int. J. Mol. Sci.* **2018**, *20*, 1, 58, DOI: 10.3390/ijms20010058
56. F. Muneer; E. Johansson; M. S. Hedenqvist; T. S. Plivelic; K. E. Markedal; I. L. Petersen; J. C. Sørensen; R. Kuktaite, *Food Res. Int.* **2018**, *106*, 607-618, DOI: 10.1016/j.foodres.2018.01.020.
57. W. R. Newson; R. Kuktaite; M. S. Hedenqvist; M. Gällstedt; E. Johansson, *J. Am. Oil Chem. Soc.* **2013**, *90*, 8, 1229-1237, DOI: 10.1007/s11746-013-2261-9.
58. W. R. Newson; R. Kuktaite; M. S. Hedenqvist; M. Gällstedt; E. Johansson, *J. Agr. Food Chem.* **2014**, *62*, 28, 6707-6715, DOI: 10.1021/jf5015928.
59. W. R. Newson; F. Rasheed; R. Kuktaite; M. S. Hedenqvist; M. Gällstedt; T. S. Plivelic; E. Johansson, *RSC Adv.* **2015**, *5*, 41, 32217-32226, DOI: 10.1039/C5RA00662G.

60. F. Rasheed; M. S. Hedenqvist; R. Kuktaite; T. S. Plivelic; M. Gällstedt; E. Johansson, *Ind. Crop. Prod.* **2015**, *73*, 90-98, DOI: 10.1016/j.indcrop.2015.04.007.
61. F. Rasheed; W. R. Newson; T. S. Plivelic; R. Kuktaite; M. S. Hedenqvist; M. Gällstedt; E. Johansson, *RSC Adv.* **2014**, *4*, 4, 2051-2060, DOI: 10.1039/C3RA45522J.
62. J. Markgren *Modeling of plant proteins in order to optimize their properties in various application*; Alnarp, 2017; p 51.
63. G. Aristippos *Protein-based films and coatings*. CRC Press, Boca Raton, **2002**, Vol. 1.
64. H. D. Belitz; W. Grosch; P. Schieberle, Amino Acids, Peptides, Proteins. In *Food Chemistry*, Belitz, H. D.; Grosch, W.; Schieberle, P., Eds. Springer Berlin Heidelberg: Berlin, Heidelberg, **2004**; pp 8-91.
65. F. Rasheed; J. Markgren; M. S. Hedenqvist; E. Johansson, *Molecules* **2020**, *25*, 4, DOI: 10.3390/molecules25040873.
66. J. Markgren; M. S. Hedenqvist; F. Rasheed; M. Skepö; E. Johansson, *Biomolecules* **2020**, *10*, 8, DOI: 10.3390/biom10081095.
67. H. Zhang; G. Mittal, *Environ. Prog. Sustain.* **2010**, *29*, 2, 203-220, DOI: 10.1002/ep.10463.
68. R. a. Markets Potato Starch Market: Global Industry Trends, Share, Size, Growth, Opportunity and Forecast 2019-2024. https://www.researchandmarkets.com/reports/4763111/potato-starch-market-global-industry-trends?utm_source=PotatoPro%20target=.
69. S. O. Kärenlampi; P. J. White, Chapter 5 - Potato Proteins, Lipids, and Minerals. In *Advances in Potato Chemistry and Technology*, Singh, J.; Kaur, L., Eds. Academic Press: San Diego, **2009**; pp 99-125.
70. A. Waglay; S. Karboune; I. Alli, *Food Chem.* **2014**, *142*, 373-382, DOI: 10.1016/j.foodchem.2013.07.060.
71. F. a. A. O. o. t. U. Nations FAOSTAT. <http://www.fao.org/faostat/en/?#data/QC>.
72. A. J. Capezza *Novel superabsorbent materials obtained from plant proteins* Sveriges lantbruksuniversitet; Alnarp, 2017; pp 1-54.
73. V. D. Capriles; J. A. G. Arêas, *Comprehensive Reviews in Food Science and Food Safety* **2014**, *13*, 5, 871-890, DOI: 10.1111/1541-4337.12091.
74. T. O. J. Blomfeldt; R. Kuktaite; E. Johansson; M. S. Hedenqvist, *Biomacromolecules.* **2011**, *12*, 5, 1707-1715, DOI: 10.1021/bm200067f.
75. S. Bräuer; F. Meister; R. P. Gottlöber; A. Nechwatal, *Macromol. Mater. Eng.* **2007**, *292*, 2, 176-183, DOI: 10.1002/mame.200600364.
76. M. Gällstedt; A. Mattozzi; E. Johansson; M. S. Hedenqvist, *Biomacromolecules.* **2004**, *5*, 5, 2020-2028, DOI: 10.1021/bm040044q.
77. I. Olabarrieta; S.-W. Cho; M. Gällstedt; J.-R. Sarasua; E. Johansson; M. S. Hedenqvist, *Biomacromolecules.* **2006**, *7*, 5, 1657-1664, DOI: 10.1021/bm0600973.

78. J. H. Woychik; J. A. Boundy; R. J. Dimler, *J. Agr. Food Chem.* **1961**, *9*, 4, 307-310, DOI: 10.1021/jf60116a020.
79. A. J. Capezza; D. Glad; H. D. Özeren; W. R. Newson; R. T. Olsson; E. Johansson; M. S. Hedenqvist, *ACS Sustain. Chem. Eng.* **2019**, *7*, 21, 17845-17854, DOI: 10.1021/acssuschemeng.9b04352.
80. I. Wojnowska; S. Poznanski; W. Bednarski, *J. Food Sci.* **1982**, *47*, 1, 167-172, DOI: 10.1111/j.1365-2621.1982.tb11051.x.
81. D.-q. Zhang; T.-h. Mu; H.-n. Sun; J.-w. Chen; M. Zhang, *Int. J. Food Prop.* **2017**, *20*, 9, 2113-2127, DOI: 10.1080/10942912.2016.1230873.
82. S. Løkra; K. Strætkvern, *Global Science Books.* **2009**, *3*, 88-95.
83. N. L. M. Grubben; L. van Heeringen; K. J. Keesman, *Potato Research* **2019**, *62*, 3, 333-344, DOI: 10.1007/s11540-019-9414-7.
84. G. A. van Koningsveld; H. Gruppen; H. H. J. de Jongh; G. Wijngaards; M. A. J. S. van Boekel; P. Walstra; A. G. J. Voragen, *J. Agric. Food. Chem.* **2001**, *49*, 10, 4889-4897, DOI: 10.1021/jf010340j.
85. W. Bergthaller; H. Themeier; M. G. Lindhauer, Wheat Gluten Modification by Alkaline Treatment and Succinylation in a Semi-technical Process. In *Plant Proteins from European Crops*, Guéguen, J.; Popineau, Y., Eds. Springer Berlin Heidelberg: Berlin, **1998**; pp 292-296.
86. A. J. Capezza; M. Lundman; R. T. Olsson; W. R. Newson; M. S. Hedenqvist; E. Johansson, *Biomacromolecules* **2020**, DOI: 10.1021/acs.biomac.9b01646.
87. O. Das; M. S. Hedenqvist; E. Johansson; R. T. Olsson; T. A. Loho; A. J. Capezza; R. K. Singh Raman; S. Holder, *Compos. Part A-Appl. S.* **2019**, *120*, 42-48, DOI: 10.1016/j.compositesa.2019.02.015.
88. O. Das; T. Loho; A. J. Capezza; I. Lemrhari; M. S. Hedenqvist, *Coatings.* **2018**, *8*, 11, 388, DOI: 10.3390/coatings8110388.
89. Q. Wu; R. L. Andersson; T. Holgate; E. Johansson; U. W. Gedde; R. T. Olsson; M. S. Hedenqvist, *J. Mater Chem. A.* **2014**, *2*, 48, 20996-21009, DOI: 10.1039/C4TA04787G.
90. Q. Wu; V. H. Lindh; E. Johansson; R. T. Olsson; M. S. Hedenqvist, *Ind. Crop. Prod.* **2017**, *97*, 184-190, DOI: 10.1016/j.indcrop.2016.12.010.
91. Q. Wu; J. Rabu; K. Goulin; C. Sainlaud; F. Chen; E. Johansson; R. T. Olsson; M. S. Hedenqvist, *Compos. Part A-Appl. S.* **2017**, *94*, 61-69, DOI: 10.1016/j.compositesa.2016.12.016.
92. Q. Wu; H. Sundborg; R. L. Andersson; K. Peuvot; L. Guex; F. Nilsson; M. S. Hedenqvist; R. T. Olsson, *RSC Adv.* **2017**, *7*, 30, 18260-18269, DOI: 10.1039/C7RA01082F.
93. Q. Wu; S. Yu; M. Kollert; M. Mtimet; S. V. Roth; U. W. Gedde; E. Johansson; R. T. Olsson; M. S. Hedenqvist, *ACS Sustain. Chem. Eng.* **2016**, *4*, 4, 2395-2404, DOI: 10.1021/acssuschemeng.6b00099.
94. A. A. Cuadri; C. Bengoechea; A. Romero; A. Guerrero, *Eur. Polym. J.* **2016**, *85*, 164-174, DOI: 10.1016/j.eurpolymj.2016.10.026.

95. A. A. Cuadri; A. Romero; C. Bengoechea; A. Guerrero, *Polym. Test.* **2017**, *58*, 126-134, DOI: 10.1016/j.polymertesting.2016.12.024.
96. A. A. Cuadri; A. Romero; C. Bengoechea; A. Guerrero, *J. Polym. Environ.* **2018**, *26*, 7, 2934-2944, DOI: 10.1007/s10924-018-1183-x.
97. A. Pourjavadi; M. Ayyari; M. S. Amini-Fazl, *Eur. Polym. J.* **2008**, *44*, 4, 1209-1216, DOI: 10.1016/j.eurpolymj.2008.01.032.
98. A. Pourjavadi; H. Hosseinzadeh; M. Sadeghi, *J. Compos. Mater.* **2007**, *41*, 17, 2057-2069, DOI: 10.1177/0021998307074125.
99. A. Pourjavadi; M. Kurdtabar; G. R. Mahdavinia; H. Hosseinzadeh, *Polym. Bull.* **2006**, *57*, 6, 813-824, DOI: 10.1007/s00289-006-0649-5.
100. B. Zhang; Y. Cui; G. Yin; X. Li; L. Liao; X. Cai, *Polym. Composite.* **2011**, *32*, 5, 683-691, DOI: 10.1002/pc.21077.
101. B. Zhang; Y. Cui; G. Yin; X. Li; Y. You, *Int. J. Polym. Mater. Po.* **2010**, *59*, 12, 1018-1032, DOI: 10.1080/00914031003760709.
102. W. Brostow; H. E. Hagg, *Materials Recycling and Sustainability*. In *Materials: Introduction and Applications*, Sons, J. W., Ed. John Wiley & Sons: New Jersey, **2017**; Vol. 1, pp 427-440.
103. D.-C. Hwang; S. Damodaran, *J. Appl. Polym. Sci.* **1996**, *62*, 8, 1285-1293, DOI: 10.1002/(SICI)1097-4628(19961121)62:8<1285::AID-APP19>3.0.CO;2-6.
104. D.-C. Hwang; S. Damodaran, *J. Agr. Food Chem.* **1996**, *44*, 3, 751-758, DOI: 10.1021/jf9503826.
105. D.-C. Hwang; S. Damodaran, *J. Am. Oil Chem. Soc.* **1997**, *74*, 9, 1165-1171, DOI: 10.1007/s11746-997-0041-0.
106. D.-C. Hwang; S. Damodaran, *J. Appl. Polym. Sci.* **1998**, *64*, 5, 891-901, DOI: 10.1002/(SICI)1097-4628(19970502)64:5<891::AID-APP9>3.0.CO;2-K.
107. G. Rathna; S. Damodaran, *J. Appl. Polym. Sci.* **2001**, *81*, 9, 2190-2196, DOI: 10.1002/app.1655.
108. G. Rathna; S. Damodaran, *J. Appl. Polym. Sci.* **2002**, *85*, 1, 45-51, DOI: 10.1002/app.10566.
109. B. S. Chiou; H. Jafri; T. Cao; G. H. Robertson; K. S. Gregorski; S. H. Imam; G. M. Glenn; W. J. Orts, *J. Appl. Polym. Sci.* **2013**, *129*, 6, 3192-3197, DOI: 10.1002/app.39044.
110. C. Demitri; R. Del Sole; F. Scalera; A. Sannino; G. Vasapollo; A. Maffezzoli; L. Ambrosio; L. Nicolais, *J. Appl. Polym. Sci.* **2008**, *110*, 4, 2453-2460, DOI: 10.1002/app.28660.
111. T. Yoshimura; K. Matsuo; R. Fujioka, *J. Appl. Polym. Sci.* **2006**, *99*, 6, 3251-3256, DOI: 10.1002/app.22794.
112. B. Alander; A. J. Capezza; Q. Wu; E. Johansson; R. T. Olsson; M. S. Hedenqvist, *Ind. Crop. Prod.* **2018**, *119*, 41-48, DOI: 10.1016/j.indcrop.2018.03.069.
113. C. Marquié, *J. Agr. Food Chem.* **2001**, *49*, 10, 4676-4681, DOI: 10.1021/jf0101152.
114. I. Migneault; C. Dartiguenave; M. J. Bertrand; K. C. Waldron, *BioTechniques.* **2004**, *37*, 5, 790-802, DOI: 10.2144/04375rv01.

115. Y. Wang; X. Mo; X. S. Sun; D. Wang, *J. Appl. Polym. Sci.* **2007**, *104*, 1, 130-136, DOI: 10.1002/app.24675.
116. A. J. Capezza; Y. Cui; K. Numata; M. Lundman; W. R. Newson; R. T. Olsson; E. Johansson; M. S. Hedenqvist, *Adv. Sustain. Syst.* **2020**, *n/a*, 2000110, DOI: 10.1002/adsu.202000110.
117. Y. Deng; W. M. J. Achten; K. Van Acker; J. R. Duflou, *Biofuel Bioprod Bior* **2013**, *7*, 4, 429-458, DOI: 10.1002/bbb.1406.
118. A. J. Capezza; E. Robert; M. Lundman; W. R. Newson; E. Johansson; M. S. Hedenqvist; R. T. Olsson, *Polymers (Basel)* **2020**, *12*, 2, DOI: 10.3390/polym12020459.
119. D. Liu; Q. Wu; R. L. Andersson; M. S. Hedenqvist; S. Farris; R. T. Olsson, *J. Mat. Chem. A* **2015**, *3*, 30, 15745-15754, DOI: 10.1039/C5TA03646A.
120. M. Salajková; L. A. Berglund; Q. Zhou, *J. Mat. Chem.* **2012**, *22*, 37, 19798-19805, DOI: 10.1039/C2JM34355J.
121. G. H. Robertson; T. K. Cao; K. S. Gregorski; W. J. Hurkman; C. K. Tanaka; B. S. Chiou; G. M. Glenn; W. J. Orts, *J. Appl. Polym. Sci.* **2014**, *131*, 2, DOI: 10.1002/app.39440.
122. Edana, Nonwovens Standard Procedures. 2015; pp 1-13.
123. S. W. Cho; M. Gällstedt; E. Johansson; M. S. Hedenqvist, *Int. J. Biol. Macromol.* **2011**, *48*, 1, 146-152, DOI: 10.1016/j.ijbiomac.2010.10.012.
124. R. Hollertz; V. L. Durán; P. A. Larsson; L. Wågberg, *Cellulose*. **2017**, *24*, 9, 3883-3899, DOI: 10.1007/s10570-017-1387-6.
125. P. S. Liu; G. F. Chen, General Introduction to Porous Materials. In *Porous Materials*, Liu, P. S.; Chen, G. F., Eds. Butterworth-Heinemann: Boston, **2014**; pp 1-20.
126. M. F. Butler; Y.-F. Ng; P. D. A. Pudney, *J. Polym. Sci. A: Polym. Chem.* **2003**, *41*, 24, 3941-3953, DOI: 10.1002/pola.10960.
127. C. Ninh; A. Iftikhar; M. Cramer; C. J. Bettinger, *J. Mater Chem. B.* **2015**, *3*, 22, 4607-4615, DOI: 10.1039/C4TB02025A.
128. F. Song; L.-M. Zhang, *Ind. Eng. Chem. Res.* **2009**, *48*, 15, 7077-7083, DOI: 10.1021/ie801372f.
129. I. A. Neri-Numa; M. G. Pessoa; B. N. Paulino; G. M. Pastore, *Trends Food Sci. Tech.* **2017**, *67*, 271-279, DOI: 10.1016/j.tifs.2017.06.018.
130. C. Chang; B. Duan; J. Cai; L. Zhang, *Eur. Polym. J.* **2010**, *46*, 1, 92-100, DOI: 10.1016/j.eurpolymj.2009.04.033.
131. J.-J. Max; C. Chapados, *J. Phys. Chem. A.* **2004**, *108*, 16, 3324-3337, DOI: 10.1021/jp036401t.
132. F.-L. Mi; S.-S. Shyu; C.-K. Peng, *J. Polym. Sci. A Polym. Chem.* **2005**, *43*, 10, 1985-2000, DOI: 10.1002/pola.20669.
133. K. C. Lanigan; K. Pidsosny, *Vibrational Spectroscopy* **2007**, *45*, 1, 2-9, DOI: 10.1016/j.vibspec.2007.03.003.
134. H. Xu; L. Shen; L. Xu; Y. Yang, *Ind. Crop. Prod.* **2015**, *74*, 234-240, DOI: 10.1016/j.indcrop.2015.05.010.

135. P. Criado; C. Fraschini; S. Salmieri; r. D. Beche; A. Safrany; M. Lacroix, *Ind. Biotechnol.* **2015**, *11*, 1, 59-68, DOI: 10.1089/ind.2014.0017.
136. A. M. Senna; K. M. Novack; V. R. Botaro, *Carbohydr. Polym.* **2014**, *114*, 260-268, DOI: 10.1016/j.carbpol.2014.08.017.
137. B. Mimouni; J. Raymond; A. M. Merle-Desnoyers; J. L. Azanza; A. Ducastaing, *J. Cereal Sci.* **1994**, *20*, 2, 153-165, DOI: 10.1006/jcrs.1994.1055.
138. K. A. Tilley; R. E. Benjamin; K. E. Bagorogoza; B. M. Okot-Kotber; O. Prakash; H. Kwen, *J. Agr. Food Chem.* **2001**, *49*, 5, 2627-2632, DOI: 10.1021/jf010113h.
139. S. Krimm; J. Bandekar, Vibrational Spectroscopy and Conformation of Peptides, Polypeptides, and Proteins. In *Advances in Protein Chemistry*, Anfinsen, C. B.; Edsall, J. T.; Richards, F. M., Eds. Academic Press: **1986**; Vol. 38, pp 181-364.
140. J. J. Nájera; A. B. Horn, *Phys. Chem. Chem. Phys.* **2009**, *11*, 3, 483-494, DOI: 10.1039/B812182F.

TRITA-CBH-FOU-2020:50
ISBN (print version): 978-91-7760-624-6
ISBN (electronic version): 978-91-7760-625-3
ISSN: 1652-6880
Serial number in the Acta-series: 2020:53